LIGHT-WEIGHT, LOW COST, HIGH-EFFICIENCY SOLAR CELLS FOR SPACE PLANAR ARRAYS

Michael L. Timmons

Research Triangle Institute
P. O. Box 12194
Research Triangle Park, NC 27709

January 1996

Final Report

Distribution authorized to DoD components only; Proprietary Information; January 1996. Other requests for this document shall be referred to AFMC/STI.

WARNING - This document contains technical data whose export is restricted by the Arms Export Control Act (Title 22, U.S.C., Sec 2751 et seq.) or The Export Administration Act of 1979, as amended (Title 50, U.S.C., App. 2401, et seq.). Violations of these export laws are subject to severe criminal penalties. Disseminate IAW the provisions of DoD Directive 5230.25 and AFI 61-204.

DESTRUCTION NOTICE - For classified documents, follow the procedures in DoD 5200.22-M, Industrial Security Manual, Section II-19 or DoD 5200.1-R, Information Security Program Regulation, Chapter IX. For unclassified, limited documents, destroy by any method that will prevent disclosure of contents or reconstruction of the document.

19960422 042
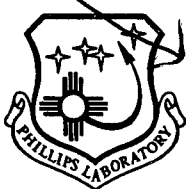
PHILLIPS LABORATORY
Space and Missiles Technology Directorate
AIR FORCE MATERIEL COMMAND
KIRTLAND AIR FORCE BASE, NM 87117-5776

AD NUMBER

AD- B209 013

NEW LIMITATION CHANGE

TO

DISTRIBUTION STATEMENT A -
Approved for public release; Distri-
bution unlimited.

Limitation Code: 1

FROM

DISTRIBUTION STATEMENT   -

Limitation Code:

AUTHORITY

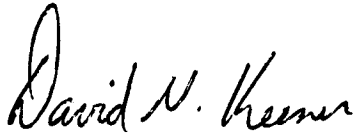Janet E. Mosher, Phillips Lab/CA, Kirtland AFB, N.M.

Using Government drawings, specifications, or other data included in this document for any purpose other than Government procurement does not in any way obligate the U.S. Government. The fact that the Government formulated or supplied the drawings, specifications, or other data, does not license the holder or any other person or corporation; or convey any rights or permission to manufacture, use, or sell any patented invention that may relate to them.

This report contains proprietary information and shall not be either released outside the government, or used, duplicated or disclosed in whole or in part for manufacture or procurement, without the written permission of the contractor. This legend shall be marked on any reproduction hereof in whole or in part.

If you change your address, wish to be removed from this mailing list, or your organization no longer employs the addressee, please notify PL/VTP, 3550 Aberdeen Ave SE, Kirtland AFB, NM 87117-5776.
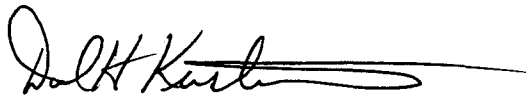
Do not return copies of this report unless contractual obligations or notice on a specific document requires its return.

This report has been approved for publication.

DAVID KEENER, Lt, USAF
Project Manager

FOR THE COMMANDER

DAVID H. KRISTENSEN, Lt Col, USAF   HENRY L. PUGH, JR., Col, USAF
Chief, Space Power and Thermal Management   Director, Space and Missiles Technology
Division   Directorate

The following notice applies to any unclassified (including originally classified and now declassified) technical reports released to "qualified U.S. contractors" under the provisions of DoD Directive 5230.25, Withholding of Unclassified Technical Data From Public Disclosure.

NOTICE TO ACCOMPANY THE DISSEMINATION OF EXPORT-CONTROLLED TECHNICAL DATA

1. Export of information contained herein, which includes, in some circumstances, release to foreign nationals within the United States, without first obtaining approval or license from the Department of State for items controlled by the International Traffic in Arms Regulations (ITAR), or the Department of Commerce for items controlled by the Export Administration Regulations (EAR), may constitute a violation of law.

2. Under 22 U.S.C. 2778 the penalty for unlawful export of items or information controlled under the ITAR is up to two years imprisonment, or a fine of $100,000, or both. Under 50 U.S.C., Appendix 2410, the penalty for unlawful export of items or information controlled under the EAR is a fine of up to $1,000,000, or five times the value of the exports, whichever is greater; or for an individual, imprisonment of up to 10 years, or a fine of up to $250,000, or both.

3. In accordance with your certification that establishes you as a "qualified U.S. Contractor", unauthorized dissemination of this information is prohibited and may result in disqualification as a qualified U.S. contractor, and may be considered in determining your eligibility for future contracts with the Department of Defense.

4. The U.S. Government assumes no liability for direct patent infringement, or contributory patent infringement or misuse of technical data.

5. The U.S. Government does not warrant the adequacy, accuracy, currency, or completeness of the technical data.

6. The U.S. Government assumes no liability for loss, damage, or injury resulting from manufacture or use for any purpose of any product, article, system, or material involving reliance upon any or all technical data furnished in response to the request for technical data.

7. If the technical data furnished by the Government will be used for commercial manufacturing or other profit potential, a license for such use may be necessary. Any payments made in support of the request for data do not include or involve any license rights.

8. A copy of this notice shall be provided with any partial or complete reproduction of these data that are provided to qualified U.S. contractors.

D E S T R U C T I O N   N O T I C E

For classified documents, follow the procedures in DoD 5200.22-M, Industrial Security Manual, Section II-19 or DoD 5200.1-R, Information Security Program Regulation, Chapter IX. For unclassified, limited documents, destroy by any method that will prevent disclosure of contents or reconstruction of the document.

DRAFT SF 298

1. Report Date (dd-mm-yy) January 1996	2. Report Type Final	3. Dates covered (from... to) 8/91 to 1/96	
4. Title & subtitle Light-Weight, Low Cost, High-Efficiency Solar Cells for Space Planar Arrays		5a. Contract or Grant # F33615-91-C-2155	
		5b. Program Element # 62601F	
6. Author(s) Michael L. Timmons		5c. Project # 2864	
		5d. Task # TG	
		5e. Work Unit # RT	
7. Performing Organization Name & Address Research Triangle Institute P. O. Box 12194 Research Triangle Park, NC 27709		8. Performing Organization Report # RTI/5122/Final-95	
9. Sponsoring/Monitoring Agency Name & Address Phillips Laboratory 3550 Aberdeen Ave SE Kirtland AFB, NM 87117-5776		10. Monitor Acronym	
		11. Monitor Report # PL-TR-96-1007	

12. Distribution/Availability Statement
Distribution authorized to DoD components only; Proprietary Information; January 1996. Other requests shall be referred to AFMC/STI.

13. Supplementary Notes

14. Abstract

The objective of this program was to produce an AlGaAs (or GaInAsP) and Si mechanically stacked tandem solar cell that meets the program goals of PRDA 91-01-PKRN POC. The band gap of the AlGaAs or GaInAsP top cell is 1.7 eV to current-match the Si bottom cell. These cells are joined by a process called eutectic metal bonding that places the two photovoltaic cells in series.

Efficiencies of the Si bottom cells exceeded 16.5 percent under AM0 illumination. However, these cells showed an unexpectedly large amount of radiation damage when the AM0 spectrum was filtered to include only wavelengths longer than 0.73 μm, duplicating the environment of a Si cell in the tandem stack. Attempts to solve this problem with higher resistivity Si wafers and variation of junction depths were only partially successful. The radiation-degradation problem remains for the Si cell.

The GaInAsP cells produced AM0 efficiencies greater than 20 percent and showed low-temperature annealing of radiation-induced damage. This cell has significant potential for space applications.

15. Subject Terms

Mechanically stacked solar cells; Silicon solar cells; GaInAsP solar cells; AlGaAs solar cells;

Radiation damage; Low-temperature annealing of radiation damage; Eutectic metal bonding

Security Classification of			19. Limitation of Abstract Limited	20. # of Pages 74	21. Responsible Person (Name and Telephone #) Lt Dave Keener (505) 846-5393
16. Report Unclassified	17. Abstract Unclassified	18. This Page Unclassified			

TABLE OF CONTENTS

LIST OF FIGURES

v

LIST OF TABLES

1.0 EXECUTIVE SUMMARY

This report describes the efforts to develop _Lightweight Low-Cost, High-Efficiency Solar Cells for Space Planar Arrays_ (Contract No. F33615-91-C-2155). This is the Final Report for the program, includes details of technical information, and covers the period from 31 August 1991 through 15 November 1995 (technical period of performance).

Program objectives were described in RTI (Research Triangle Institute) Proposal No. P831-010, submitted in response to PRDA 91-01-PKRN POC. To meet PRDA efficiency, weight, cost, radiation degradation, high-temperature exposure, terminal connection, and space qualification requirements, RTI began developing a mechanically stacked tandem solar cell.

The bottom cell in the stack is a high-efficiency Si cell, fabricated by ASEC (Applied Solar Energy Corporation), RTI's partner in this program. Stand-alone Si cells from ASEC demonstrated efficiencies greater than 16.0 percent during the course of the program using conventional processing. The final target efficiency was 18 percent, to be accomplished using advanced processing such as that being developed by the photovoltaic group at the University of New South Wales, Sydney, Australia.

To match the current of a Si cell, top cells made of either AlGaAs or GaInAsP alloys (alloy compositions with band gaps of about 1.7 eV) were grown and fabricated by RTI. These cells were to be thinned and mechanically stacked onto the Si cell using a process developed at RTI called EMB (eutectic metal bonding). In the program, AlGaAs cells achieved efficiencies as high as 17 percent, and GaInAsP cells attained 20 percent. GaAs wafers were bonded to Si wafers with EMB and survived cycling between liquid nitrogen and boiling water without wafer delamination. This temperature cycling demonstrates the strength of joints formed by the EMB process although the work was terminated before any stacked cells could be tested. Thin AlGaAs layers were bonded to Si, providing a proof of concept.

Individual component cells, as well as completed cells, were to undergo radiation testing and space qualification. The radiation testing (1 MeV electrons at a fluence of 10^{15} cm^{-2}) uncovered a major problem for Si cells in the context of the structure being developed. Under a GaAs wafer, which filters the high energy photons as a high-band-gap cell would in a tandem stack, standard Si cells degraded more dramatically than under a full spectrum. In fact, under the truncated AM0 spectrum, the EOL/BOL current ratio of Si falls from 0.74 to 0.45. Spectral response data clearly show the Si cells are susceptible to degradation at longer wavelengths. This problem is fundamentally related to the relationship between the absorption of radiation and diffusion length and is likely to be more severe as the efficiency of a low-band-gap cell increases, i.e., as the diffusion length becomes longer and more subject to degradation.

The radiation resistance of the GaInAsP met expectations, both showing EOL/BOL efficiency ratios greater than 0.8. The GaInAsP exhibits low-temperature an-

1

nealing of some of the radiation-induced damage, similar in behavior to InP but to a lesser extent. This behavior was an unexpected benefit for GaInAsP.

The second major problem encountered during the effort is the ability to grow AlGaAs cells reproducibly well. Al-containing compounds are particularly sensitive to oxygen and water vapor contamination because the Al-O bond is very strong. For an AlGaAs solar cell, oxygen contamination introduces deep levels in the material that act as nonradiative traps, enhancing Shockley-Read-Hall (SRH) recombination limits to minority-carrier lifetime.

GaInAsP cells have a drawback also. To lattice-match Ge and GaAs substrates, upon which the GaInAsP is grown (prior to substrate removal), requires control of four source gases that have different decomposition profiles and vapor pressures. This is not a trivial task even in a small reactor. Looking toward manufacturing where control in large production-sized reactors are paramount issues, we elected to focus on the Al-GaAs cells for the top cell in the structure under development. This decision was made regardless of better performance from GaInAsP cells.

The program was truncated at the end of Phase II (of a three-phase program) for two reasons: (1) funds limitations and (2) progress made with the $Ga_{0.5}In_{0.5}P$/GaAs monolithic tandem cell in another PRDA programs. The final work on this program focused on evaluating a TMA (trimethylaluminum) source that is believed to have the potential to improve the quality of AlGaAs cells and to enable AlGaAs to be grown at lower temperatures than is normally required. If successful, this TMA source has the potential to make an AlGaAs/GaAs monolithic cell competitive with the GaInP/GaAs one, and there are manufacturing factors that favor the AlGaAs/GaAs.

2.0 INTRODUCTION

This report, the Final Report for Contract No. F33615-91-C-2155, presents the details of experimental work conducted during the program's duration. The effort was originally funded out of the Wright Laboratory, Wright-Patterson AFB, OH, but was transferred to Phillips Laboratory, Kirtland AFB, NM, shortly after it began. This transfer caused a 6-month interruption in the effort. There was also an interruption in the program when Phase II funding was depleted, and the program was descoped to evaluations of a TMA source and AlGaAs cells grown with this TMA. All delays combined extended the period of performance to 15 November 1995 from 31 August 1991.

2.1 Technical Objectives

The technical objectives the this program to develop *Lightweight, Low-Cost, High-Efficiency Solar Cells for Space Planar Arrays* are found in PRDA 91-01-PKRN POC and are summarized as follows:

- <u>Efficiency</u>. The cell efficiency must be ≥ 23 percent (AM0) at 30 to 50°C. The program efficiency goal is 30 percent (AM0).

- <u>Weight</u>. The cell must be lightweight. When mounted on a lightweight, rigid aluminum honeycomb structure, the module specific power must be > 80 W/Kg. For 23-percent efficiency, the specific power implies an overall density for the cell/module combination of less than 390 mg/cm^2.

- <u>Cost</u>. The cell cost should be low. The advanced technology used must provide cost-effective producibility.

- <u>Radiation Degradation</u>. The maximum power of the cells should not decrease by more than 20 percent after exposure to 1 × 10^{15}, 1-MeV electrons/cm^2.

- <u>High Temperature Exposure</u>. The cell must withstand temperature cycling to 425°C without significant degradation.

- <u>Terminal Connections</u>. The cell must have two terminals and must be easily integrated into present-day arrays.

- <u>Qualification Tests</u>. Cell performance must be acceptable after exposure to qualification tests, including radiation, thermal cycling, contact/interconnect pull strength, humidity/temperature, temperature characterization, and exposure to high temperatures.

These are a demanding set of requirements. A plan to meet these technical objectives, offered in RTI's proposal response to the PRDA solicitation, is set forth in the next section.

2.2 Approach to Achieve PRDA Program Goals

Philosophically, in responding to the PRDA solicitation, RTI felt that there were two approaches with the best chance to meet the goals. The first is a monolithic tandem cell consisting of a high-band-gap junction made of $Al_xGa_{(1-x)}As$ or $Ga_{0.5}In_{0.5}P$ (hereafter call AlGaAs and GaInP, respectively, unless reference is made to a specific alloy composition), The low-band-gap junction would be GaAs in this structure, and growth would employ a Ge substrate. Our preliminary modeling showed that this structure has the potential to achieve an efficiency of about 25 percent under AM0 illumination. Subsequent work by Bertness et al. [1] resulted in a GaInP/GaAs that achieved the modeled efficiency in small-area cells. And quite frankly, results with this cell progressed much faster than we anticipated.

The fundamental problem with an AlGaAs/GaAs or a GaInP/GaAs cell is that the band gaps are too high to make maximum use of the solar spectrum, i.e., the efficiencies are limited because photon utilization is incomplete. To overcome this problem, the band gaps need to be lowered. Modeling [2] shows that the optimum band gaps for a two-junction cell under AM0 illumination are about 1.1 and 1.7 eV for the bottom and top junction, respectively, with a potential efficiency over 30 percent. This band-gap pair forms the basis for the approach a team consisting of RTI and ASEC proposed to meet the PRDA requirements with more engineering margin than the higher band-gap pair provides.

The proposed program pulls from the strength of both team members. ASEC has been fabricating and providing Si solar cells that are fully space qualified for a number of years. Si has the desired low band gap for the cascade pair but is also the cheapest, most lightweight, most available, and most rugged of all solar cells currently in widespread use. It is the logical low-band-gap choice for the structure that was proposed. ASEC-produced Si cells reached a 16.5-percent efficiency during the program, and at termination, more advanced processing offered the potential to reach 18 percent. Stand-alone cell efficiencies between 16 and 18 percent are essential since the bottom cell in a stack is expected to produce about 8 or 9 percent, and cell currents in a stack are about one half of those in a free cell (thereby cutting efficiency in half). Results of the Si work are described in detail in Section 3, which follows.

RTI's contributions to the program began with the top-cell technology. To provide a cell with a 1.7-eV band gap, two materials were considered. The first is $Al_{0.2}Ga_{0.8}As$, and the second is $Ga_{0.7}In_{0.3}As_{0.4}P_{0.6}$. Both lattice-match GaAs and Ge substrates. RTI brought considerable experience in both materials systems to this research effort. With either of these materials, we expected efficiencies of at least 18 percent and more optimistically of 20 percent, giving a stack efficiency potential of pos-

4

sibly as much as 28 or 29 percent. Details of work with both AlGaAs and GaInAsP can be found in Section 4.

RTI also had developed the final piece needed for the structure, a means of joining Si and III/V materials such as GaAs. The method, called EMB has been shown to allow thin GaAs layers to be joined to Si with essentially no strain [3]. Using TPL (transient photoluminescence), Dr. R.K. Ahrenkiel estimated that the minority-carrier lifetime in 6-μm-thick GaAs layer exceeded 100 ns, suggesting that these thin III/V layers would have more than adequate diffusion lengths for high-efficiency solar cells. Details of cell bonding are located in Section 5.

The program approach, then, was to grow thin AlGaAs or GaInAsP cells, bond these cells to a fully processed Si cell with EMB, remove the original substrates used for the III/V growth, and complete the cell processing of the III/V material bonded to the Si.

This program, if successful, would have met all technical goals of the PRDA solicitation. The cell cost goals would be evaluated as cost issues were identified, and scale-up plans to manufacturing quantities were to be developed. The program contained, in short, a solid technological base from a team of well-blended research and manufacturing personnel.

In the sections that follow, the technical details are presented. Included are details of the problem areas—Si radiation resistance and AlGaAs cell reproducibility—that made progress difficult. We conclude this report with recommendations for future research.

3.0   DEVELOPMENT OF SI JUNCTIONS

3.1   Introduction

In this section, the details of the work ASEC completed with the Si bottom cell are found. The effort includes demonstration of cell efficiencies greater than 16.5 percent under AM0 illumination, exceeding a Phase I goal of 16 percent. A problem with Si radiation resistance under a truncated AM0 spectrum was identified during irradiation testing of cells. Attempts to modify the Si structure to improve EOL performance are described.

3.2   Si Cell Structures

3.2.1   Baseline Cells

The baseline cells used for this program are similar to standard production cells being manufactured but with some modifications of the surfaces to increase performance. These cells were fabricated from p-type Si slices using double diffusion to form a p^+ region at the rear of the device that acts as a back surface field. The second diffusion, using P, forms an n^+ region at the front, yielding an $n^+/p/p^+$ structure. The P diffusion is shallow, forming a junction about 0.2 μm deep. The resistivity of the Si is 0.2 ohm-cm.

The front surface (the cell's emitter) undergoes subsequent processing to form a passivated emitter solar cell (PESC) that contains the following features:

- front surface texturing,
- a two-layer AR (antireflective coating),
- front-surface passivation, and
- a back-surface reflector.

The grids for these devices are located on flat areas that were masked during the texturing of the surface, and grid spacing is closer than for most Si space cells to reduce contact resistivity when Si and AlGaAs (GaInAsP) are bonded together. The PESC design was selected because the technology is compatible with present space cell manufacturing technology, has the possibility of reasonably low cost, and can meet space qualification requirements in all areas (except for severe radiation conditions).

The enhanced output of these cells, compared to non-PESC production cells, results from a combination of increased minority-carrier lifetime (and, therefore, diffusion length) and light trapping (because of back reflector), giving higher currents. Pas-

sivation of the external surfaces leads to reduced recombination, providing higher voltages (lower dark currents).

Preliminary estimates (see below) of the output of these cells, when placed under a truncated AM0 spectrum with wavelengths shorter than 730 nm removed, show that the Si cell should generate about 20 mA/cm^2. Planned improvement to these cells to attain the 22-mA/cm^2 current density goal were changed after radiation testing of the first cell batch showed a significant degradation of current in the spectral region of interest.

Improvements planned for the cells come from the advanced processing being developed by the research group of the University of New South Wales, Sydney, Australia, under the direction of Dr. M. A. Green. This group has made impressive improvements in terrestrial Si-cell efficiencies. These improvements include improved texturization schemes to get more light into the device, thinner structures that use more efficient light trapping than the baseline cells, and better surface passivation to reduce dark currents even further. These improvements were not included in any cells tested for radiation degradation.

3.2.2 Cell Modifications After Radiation Testing

As a result of the data produced during radiation testing of the baseline cells, ASEC fabricated other Si structures that used substrates as thin as 50 µm (2 mils), junctions as deep as 0.7 µm, and substrate resistivities as great as 10 ohm-cm. These cells were fabricated to evaluate potential improvements in the radiation resistance of the baseline cells. The rationale for these structural changes is the following: the heavily doped Si wafers will be more susceptible to degradation of the diffusion length, and a shallow junction exacerbates the problem of poorer current collection. Hence, by making cells thinner with deeper emitters in more lightly doped substrate material, current collection after irradiation should improve. Lower BOL efficiencies may be the cost of these EOL improvements.

Of these changes, probably the most important is the base layer thickness. As base layer thickness is reduced, the absorption, particularly of the longer wavelengths is reduced; so, it is essential that internal light trapping (using the back-surface reflector) be effective to make the reflected light pass through the cell a second time. This approach increases the optical thickness of a cell by a factor of two but also requires very good passivation of the back surface to keep carrier recombination low.

A final Si modification was considered and modeled to determine options for the stack. Since the cells of this program are in a mechanical stack, more flexibility in design exists compared to a monolithic cell. By stacking a top cell on a larger bottom cell, several things could be accomplished. First, top cells can be made to limit BOL currents. Therefore, at EOL the currents can match since the bottom cell degrades more rapidly than the top cell. The bottom cell also sees some of the short-wavelength photons not masked by the top cell, perhaps yielding greater EOL currents in the Si. We

considered two cases for Si cells with increased areas using the modified production devices described above as the performance model to predict efficiencies.

1. By making the Si bottom cell 22 percent larger than an AlGaAs top cell, the current densities of the two cells match at BOL. This structure projects a BOL efficiency of between 24 and 25 percent, meeting the program goal, but the EOL/BOL ratio is likely to be no more than 0.62, short of the 0.8 specified in the requirements.

2. If the area of the Si were increased even more, by about 48 percent compared to the top cell, cell currents can be made be made to match at EOL. This change decreases BOL efficiency to about 20 percent but raises EOL to 15 percent, giving an EOL/BOL ratio of 0.75.

The results of modeling of equal cell areas and variable bottom-cell areas are summarized in Table 3.1.

Table 3.1. Modeled AlGaAs/Si Stacked Tandem Cell Efficiencies Using Equal Areas And Oversized Si Bottom Cells To Compensate For Poor Radiation Resistance Of Si To Long Wavelengths.

Stacked Cell Structure	Stack BOL Efficiency	Stack EOL Efficiency	EOL/BOL Ratio	Remarks
A. Equal area AlGaAs and Si as tested in preliminary radiation testing	18.9 %	7.5%	0.40	BOL low; EOL/BOL ratio low
B. Equal area AlGaAs and Si with J_{sc} of Si improved 3 mA/cm^2 to current match at BOL	22.8%	9.1%	0.40	BOL marginal; EOL/BOL ratio low
C. Si cell area increased by 22% to current match at BOL using cells like those in A.	24.1%	14.9%	0.62	BOL meets spec.; EOL/BOL ratio still low
D. Si cell are increased by 48% to current match the AlGaAs at EOL using cells from A.	19.9%	15.1%	0.76	BOL low; EOL/BOL ratio marginal

The modeled data in Table 3.1 show that this approach of varying the Si cell area comes close to meeting the EOL/BOL ratio but cell efficiencies must be improved in either case—equal cell areas or oversized Si cells—if BOL efficiencies and EOL/BOL ratios are to be met simultaneously. This approach might be an interesting avenue to pursue in the future but did not seem to offer enough to make it a part of this program. These results clearly point to one important factor. These cells, and perhaps all tandem cells that have component cells degrading at different rates when subjected to irradia-

tion, need to be designed for either BOL or EOL current matching. This choice should be dictated by the mission requirements and expected radiation problems.

3.2.3 Effect of Cell Thickness and Junction Depth on BOL Performance

The first irradiation of Si identified a problem at long wavelengths for the baseline cells. Since baseline cells are about 200 μm thick, with shallow, 0.2-μm junction depths, we needed to examine cells with other dimensions of thickness and junction depth to determine the effects of these parameters on current collection. ASEC produced a series of Si cells with nominal thicknesses of 50, 100, and 275 μm (2, 4, and 11 mils; 1 mil $\approx$ 25 μm) and junction depths of 0.2 and 0.7 μm. These cells were fabricated from Si with a resistivity of 10 ohm-cm, rather than 0.2 ohm-cm used for the baseline cells. Regardless of EOL performance, these cells must have reasonably good BOL performance to meet the program BOL efficiency requirement. The BOL efficiency and current are shown graphically in Figure 3.1.
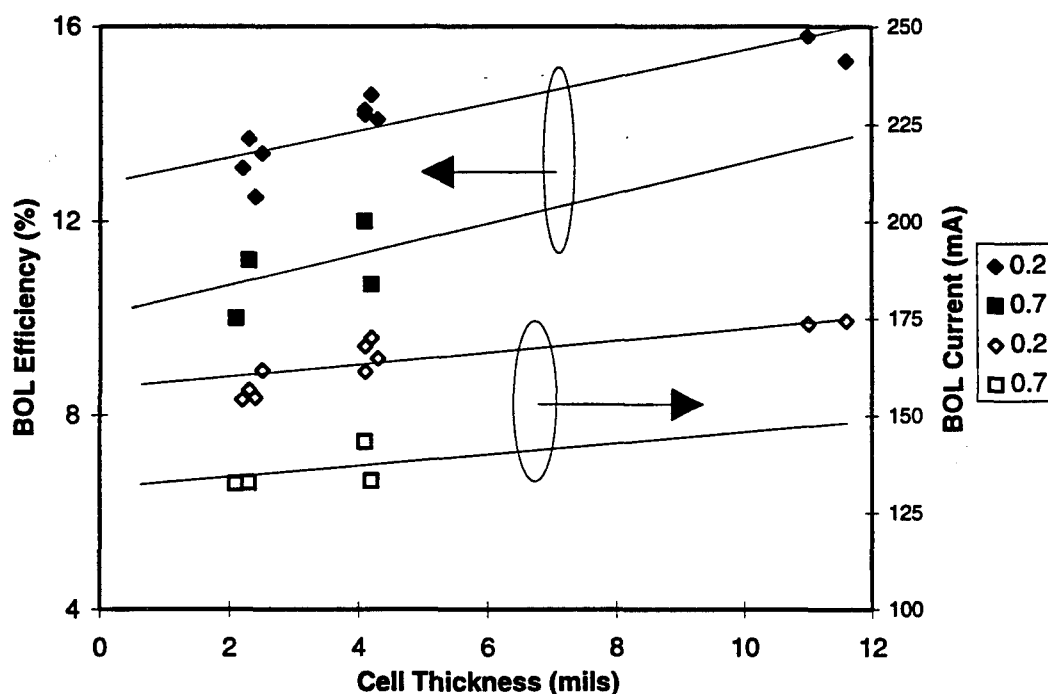
Figure 3.1. BOL efficiency and current of 4 cm^2 Si solar cells. Junction depths of 0.2 and 0.7 μm were used for the devices. Closed symbols show BOL efficiency; open symbols show BOL current.

9

The BOL efficiency drops off as cells get thinner. The thinnest cells are in the range of 13 to 14 percent for shallow junctions. This efficiency will not be sufficiently high to meet the stack BOL efficiency needs, but if the EOL efficiency is also high, the EOL/BOL ratio may meet requirements.

Much of the decrease in efficiency for the thinner cells comes from lower currents, also indicated by the data. Currents in these cells can be increased if the BSF (back-surface-field) layer is added, and improving the back-surface reflector should make a substantial improvement in the current. In addition, surfaces were not textured, but they were left rough after sawing. Making all of these improvements will undoubtedly reduce current losses. The thin cells, using high resistivity substrates, actually project efficiencies more than 16 percent when fully optimized. However, determining the radiation characteristics was more important for these cell.

These cells were irradiated and the data are reported in Section 3.4 and showed improved EOL/BOL ratios in the long-wavelength regime.

To produce these thin cells, ASEC developed a thinning process. This process has the following steps:

1. Begin with 4-mil (100 μm) Si slices and diffuse the n^+ layer.
2. Apply the grid and AR coating to complete front-side processing.
3. Mask front surface with mylar tape with UV-sensitive adhesive (to protect surface during thinning.
4. Thin wafer with HF:HNO_3 solution
5. Apply SiO_2 passivating layer and backside metallization (grid and reflecting layer).
6. Remove mylar tape by irradiating cell with UV illumination.

This process can reliably and reproducibly thin Si wafers and may be useful for other devices or applications.

3.2.4 Si Cell Polarity

The Si cells that ASEC manufactures, including the modified ones being made for this program, use the n-on-p device polarity. There is an *a priori* reason to believe that the n/p polarity will have superior radiation resistance to a p/n device: the electron mobility in a p-type base is greater than the hole mobility in an n-type base, suggesting longer diffusion lengths in n/p ones. ASEC fabricated several p/n devices, but none met the Phase 1 efficiency goal of 16 percent. Because of this relatively poor BOL performance, these p/n Si cells were not irradiated, and we decided not to allocate additional contract resources to the development of p/n Si cells.

The result had a significant impact for the program: *Since we were, in essence, fixing the bottom-cell polarity to n/p, we also fixed top-cell polarity to the same in the series-connected device.*

Unfortunately, most of the AlGaAs top cells, including those that met the Phase 1 efficiency goals, have p/n polarity. Developing the n/p AlGaAs cells has been considerably more difficult, as will be described in Section 4.

3.3 Si Cell Electrical and Spectral Characteristics at BOL

ASEC has been a major supplier of space-qualified Si solar cells for many years. In this program, some of the better 2 cm $\times$ 4 cm modified production cells were selected, and their I-V characteristics were evaluated. The best of these demonstrated an efficiency above 16.5 percent, measured under a two-source simulator at ASEC. Cells flown on the JPL balloon experiment serve as the reference standard for setting simulator intensity.

The I-V curve for two good baseline cells are shown in Figure 3.2. These cells exceeded the Phase I goal of 16 percent and showed that attaining the 18 percent efficiency desired for the final cell design (under a full AM0 spectrum) is a reasonable goal. The 16.5-percent efficiency comes from the modified production-line cell, described above, that uses a p^+ rear diffusion and a shallow n^+ diffusion into 0.2 ohm-cm material. All processing, including the two-layer AR coating, is standard for space-qualified cells that ASEC manufactures.

A typical Si cell spectral response, measured in A/W at JPL, for these devices is shown in Figure 3.2 under a full AM0 spectrum. Since the top cell of the tandem stack has a band gap of about 1.70 eV in the structure, the AM0 spectrum can be split at about 730 nm to determine the current that should be generated by the Si cell using the spectral response from 730 nm to the band edge (1.1 μm). If there is complete photon absorption in the top cell, only these longer-wavelength photons reach the Si. With this approach, a short-circuit current density J_{sc} of 20 mA/cm^2 was estimated for the spectral response pictured by convoluting the spectral response with the AM0 spectrum truncated at 730 nm. This value is lower than the 22 mA/cm^2 predicted for the AlGaAs/Si tandem stack and shows the need for improvements for Si to meet program efficiency goals. However, recall that these are modified production cells, and no rigorous optimization had been attempted. So, achieving close to 20 mA/cm^2 was certainly a favorable beginning with which we were pleased.

RTI provided ASEC with thin layers of $Al_{0.2}Ga_{0.8}As$ to use as filters when evaluating Si cells, thus putting the Si in a configuration that closely resembles the mechanical stack. Both sides of the $Al_{0.2}Ga_{0.8}As$ have AR coatings to reduce current losses in the Si. Amyl alcohol is used to optically couple the two cells, providing index matching.

It is important to understand how the Si cells respond under the $Al_{0.2}Ga_{0.8}As$ filters since that is the environment Si will see in the final device. To put bounds on cell

11

performance for shallow and very deep emitters, ASEC processed a device from a slice of Si that was thinned to about 75 μm (2.5 mils). Front processing was standard (n$^+$ diffusion, AR coating, metallization), but the backside of the device also received a

(A)

(B)
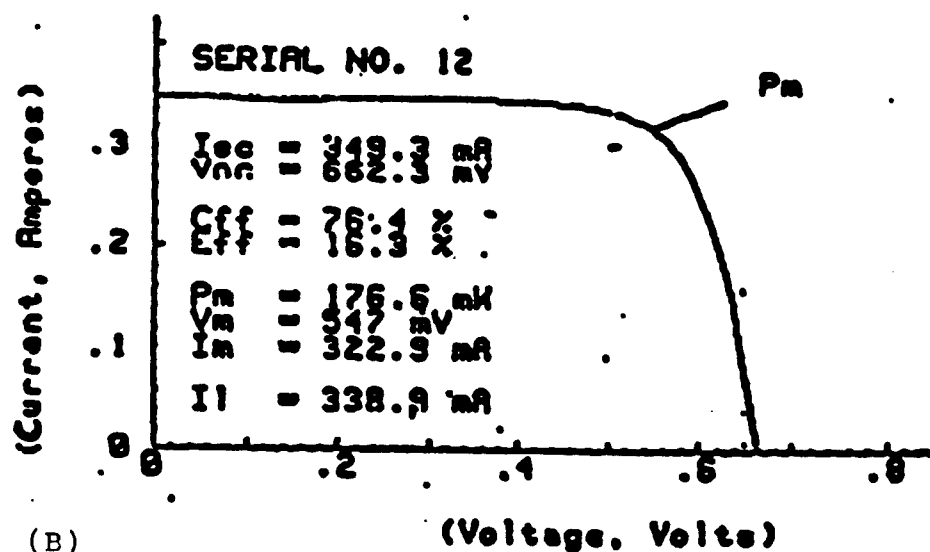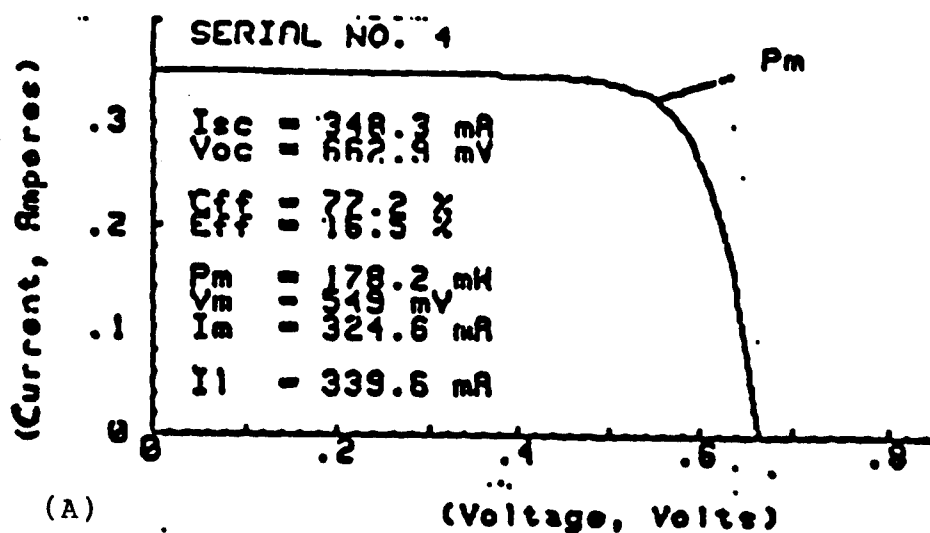
Figure 3.2. Illuminated I-V characteristic of two baseline Si cells: (a) this cell was one of the best produced in Phase I of the program with an efficiency of 16.5 percent, and (b) is another good cell more typical of the devices with an efficiency of 16.3 percent.
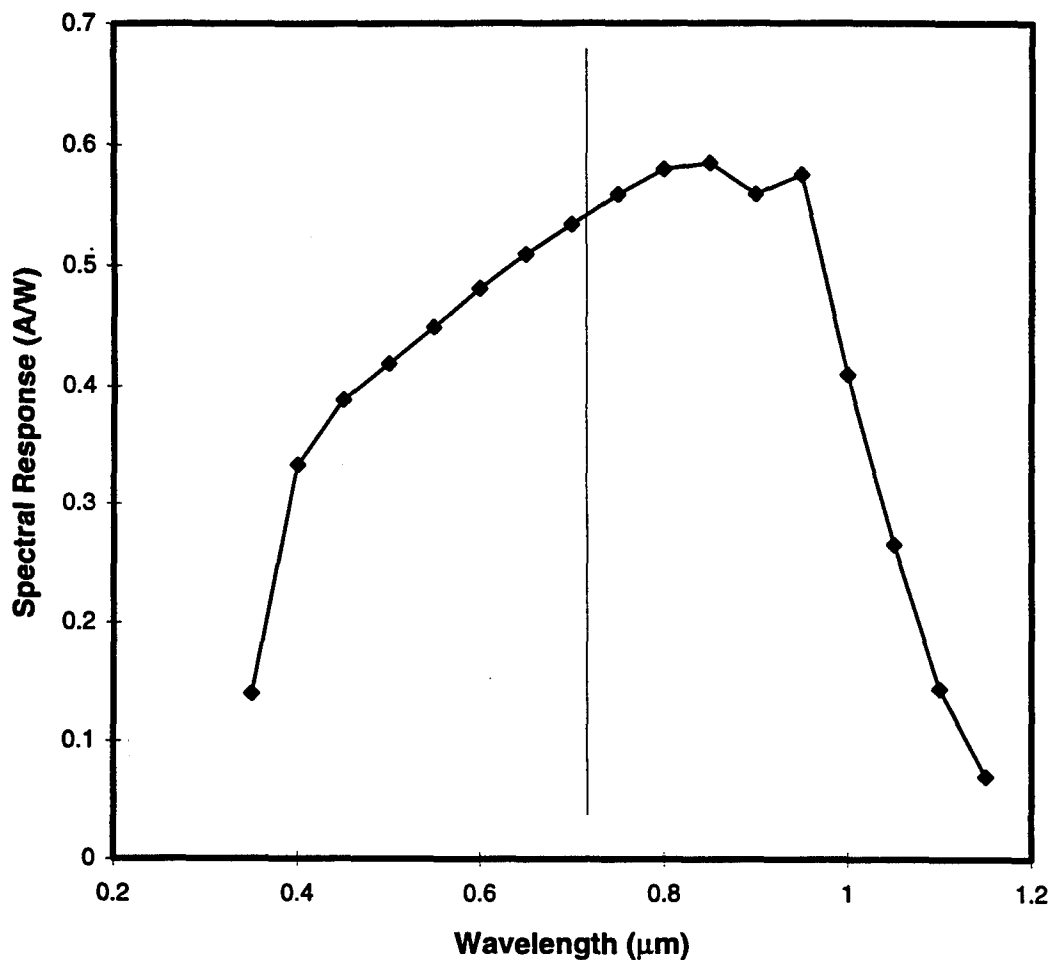
Figure 3.3. Spectral response of Si solar cell. The device was measured at JPL and is typical of most high-quality Si cells. Eliminating wavelengths equal to or less than 0.73 μm in the AM0 spectrum and convoluting that spectrum with this spectral response gives a J_{sc} of about 19 mA/cm^2 for the cell. The vertical line shows the 0.73-μm-wavelength cutoff.

metal grid and an AR coating after the p$^+$ diffusion. The AR coating on the backside of the device matches the longer wavelengths that a Si cell will see beneath an AlGaAs cell. Illuminating from the front of the device gives a standard measurement, but illumination from the backside gives the effect of a junction that is almost the depth of the wafer thickness. Data for the cell using both illuminations are shown in Table 3.2 both with and without the AlGaAs filter.

Table 3.2. I-V Characteristic of Si Solar Cell Illuminated From Both Front and Rear

Configuration	Without AlGaAs Filter				Under AlGaAs Filter			
Measured	V_{oc} (mV)	I_{sc} (mA)	FF (%)	Eff. (%)	V_{oc} (mV)	I_{sc} (mA)	FF (%)	Eff. (%)
Normal Cell	614	155	77.2	13.6	580	54.1	76.4	4.5
Deep Emitter	600	116	77.0	9.8	564	37.0	76.7	3.0

The interesting thing about these data is that the voltage of the normal configuration is only about 15 mV higher than the deep-emitter configuration. In both cases, the voltage dropped about 35 mV under the filter. Therefore, if the starting voltage of the Si cell is about 660 mV (higher than the 614 mV shown in Table 3.2), we should achieve at least 600 mV under and AlGaAs cell even with a very deep junction. This observation is important because we modeled the bottom cell to deliver 600 mV when projecting BOL efficiencies. The junction depth has little impact on the current ratios of filtered and unfiltered illumination, and fill factors are essentially unchanged.

Finally, ASEC has shown another reason besides radiation resistance to use the higher resistivity Si wafers for the bottom cells. Tests showed that under the AlGaAs filter, V_{oc} decreased faster than expected. Changes in the diode ideality factor are likely responsible at the reduced current levels filtering produces. The V_{oc} of a cell is classically described by:

$$V_{oc} = \frac{nkT}{q} \ln \frac{J_{sc}}{J_o}$$

As the current in the cell drops, the ideality factor begin to change from near 1 to 2, giving an increased voltage drop because of the larger relative dark current. In most of ASEC's experience, this has always been a greater problem for low-resistivity Si.

Radiation testing identified the key problem with the Si cells in the mechanical stack, and radiation work is described next.

3.4 Si Cell Radiation Testing

Radiation testing of high-efficiency baseline Si cells was the most important early part of the program. Not only did the test help confirm the relatively poorer radiation

resistance of Si (compared to GaAs), but it also showed surprising new and promising results for the GaInAsP cells. All irradiation was performed at the JPL facility under the direction of Dr. B. Anspaugh.

Two of the best Si cells were irradiated along with GaInAsP junctions. The pre- and post-irradiation data are shown in Table 3.3. It is important that the highest effi- ciency cells were used for the test because radiation damage generally identifies itself more clearly as cell efficiencies increase, i.e. cells with low starting efficiencies usually show smaller radiation effects. Cell areas are 8 cm^2.

Table 3.3 Current-Voltage Characteristics of Si Solar Cells Before and After Irradia- tion With 1-MeV Electrons (10^{15} cm^2).

Cell No.		V_{oc} (mV)	EOL/BOL Ratio	I_{sc} (mA)	EOL/BOL Ratio	FF (%)	EOL/BOL Ratio	η (%)	EOL/BOL Ratio
11	Before	660	0.876	347.8	0.740	78.4	0.980	16.6	0.640
	After	578		257.5		77.0		10.6	
14	Before	661	0.873	350.8	0.738	78.4	0.980	16.8	0.630
	After	577		258.9		76.8		10.6	

The EOL/BOL ratio of current is the parameter to focus on in considering these data because the efficiency ratio is essentially that seen for any good Si device. Con- sider cell number 14 as a typical device. As described in the last section, if the spectral response is convoluted with the truncated AM0 spectrum ($1.1 \geq \lambda \geq 0.73$ μm), the BOL current density should be about 17.4 mA/cm^2, but the EOL density is only 7.75 mA/cm^2. This gives an EOL/BOL ratio of 0.45, not 0.74. By filtering most of the more energetic photons, we place the burden of current collection on the base since longer wave- lengths of light penetrate more deeply in the material. Therefore, any degradation of the diffusion length with the skewed spectrum makes a significant impact on current.

The effect can be seen quite graphically in the spectral response of this cell measured both before and after irradiation. Figure 3.4 shows this quite clearly and gives a comparison of a Si cell to one of the GaInAsP cells (sample no. 6-628-8) that showed good resistance to radiation damage.

This is the crux of the problem. For longer wavelengths, the baseline Si cell shows much more degradation than for short wavelengths. Unfortunately, the cell in the mechanical stack will see only photons in this sensitive spectral region. Hence, we concluded early on that the baseline cell does not have a remote chance of meeting the EOL/BOL efficiency ratio requirement for the program. There was no choice for the Si but to investigate the other structures, the thinner cells with variable junction depths, in hopes that these structures would improve long-wavelength response.
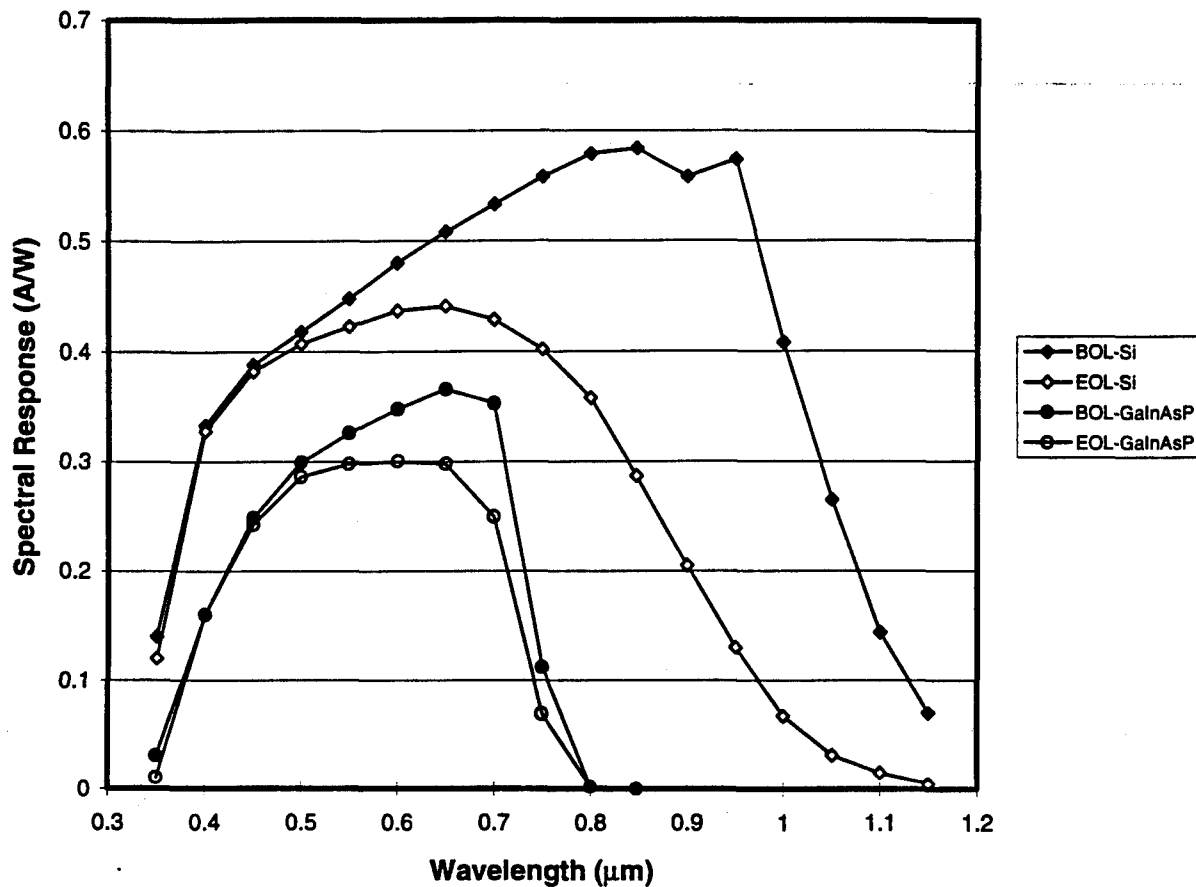
Figure 3.4. Spectral response curves measured at BOL and EOL before and after irradiation with 10^{15},1-MeV electrons/cm^2. Irradiation performed at JPL facility.

As mentioned in previous sections, several different Si structures were evaluated to improve the radiation resistance. While awaiting delivery of the 10-ohm-cm Si slices (Czochralski Si grown in the presence of a magnetic field to reduce turbulence in the molten Si) from which those devices were to be fabricated, ASEC performed a very quick experiment that suggested potentially better radiation properties. From pieces similar to the ones ordered, two devices were fabricated with shallow emitters. One piece is 200 μm (8 mils) and the other is 75 μm (3 mils). The BOL and EOL currents (irradiated with 10^{15}, 1 MeV electrons/cm^2) were measured under ASEC's two source simulator. This simulator has both W (tungsten) and Xe (xenon) lamps. The W lamp is filtered to eliminate wavelengths shorter than 0.65 μm. By estimating the amount of current generated between 0.65 and 0.73 μm and subtracting that value from the cell current measured under the W lamp, we arrive at a reasonably good approximation to

16

the truncated spectrum incident on the Si cells. This process was used to evaluate the cell currents here. The results are shown in Table 3.4.

Table 3.4. BOL and EOL Currents for Si Solar Cells Measured Under Two-Source Simulator with Both Lamps and Each Lamp Separately.

Cell Type	BOL Current Density (mA/cm^2)				EOL Density Current (mA/cm^2)			
	Both Lamps	Xe Lamp	W Lamp	$\lambda \geq 0.73$ μm	Both Lamps	Xe Lamp	W Lamp	$\lambda \geq 0.73$ μm
0.2 Ω-cm, 8 mils	43.5	19.0	24.5	17.4	32.4	17.3	15.1	7.75
10 Ω-cm, 8 mils	42.2	17.4	24.8	17.2	34.6	16.7	17.9	9.2
10 Ω-cm, 3 mils	40.2	17.2	23.0	16.3	36.1	16.7	19.4	10.0

Note: Current estimated from W measurement for wavelengths longer the 0.73 μm

The last two cells show significantly improved EOL/BOL current ratios, compared to the first cell which was from the first batch irradiated. The data from Table 3.4 are presented in bar graph format in Figure 3.5 to show these improvements graphically.

The EOL/BOL ratio for the 10 ohm-cm, 75-μm cell improved from 0.45 to 0.61 for $\lambda \geq 0.73$ μm. This is a significant improvement and gives reason to hope that for cells with more optimum parameters, for example, junction depths, needed EOL/BOL ratios will at least be approached.

Finally, the last effort in the program with the Si cells was the fabrication, irradiation, and evaluation of the Si cell variations similar using the high resistivity Si. The I-V data for these cells are shown in Table 3.5. The cells were measured under two simulators, a xenon-lamp simulator and a two-source simulator, at ASEC. Under the two source simulator, the total current under both lamps and the current under each lamp, Xe and W, were measured. The cell thicknesses and junctions depths are also included in the information in Table 3.5. The BOL efficiencies and currents of most of the cells are given in Figure 3.1.

Several comments are in order about the cells and the testing. The cells, conventional in design, were randomly selected from the matrix of cells that ASEC fabricated. They represent the nominal 50- and 100-μm (2- and 4-mil, respectively) cells. Two, 275-μm (11-mil) cells, similar to those irradiated previously, and a group of 82.5-μm (3.3 mil) cells were added as controls. Nominal junction depths are 0.2 and 0.7 μm.

Irradiation was done at JPL in a single dose.
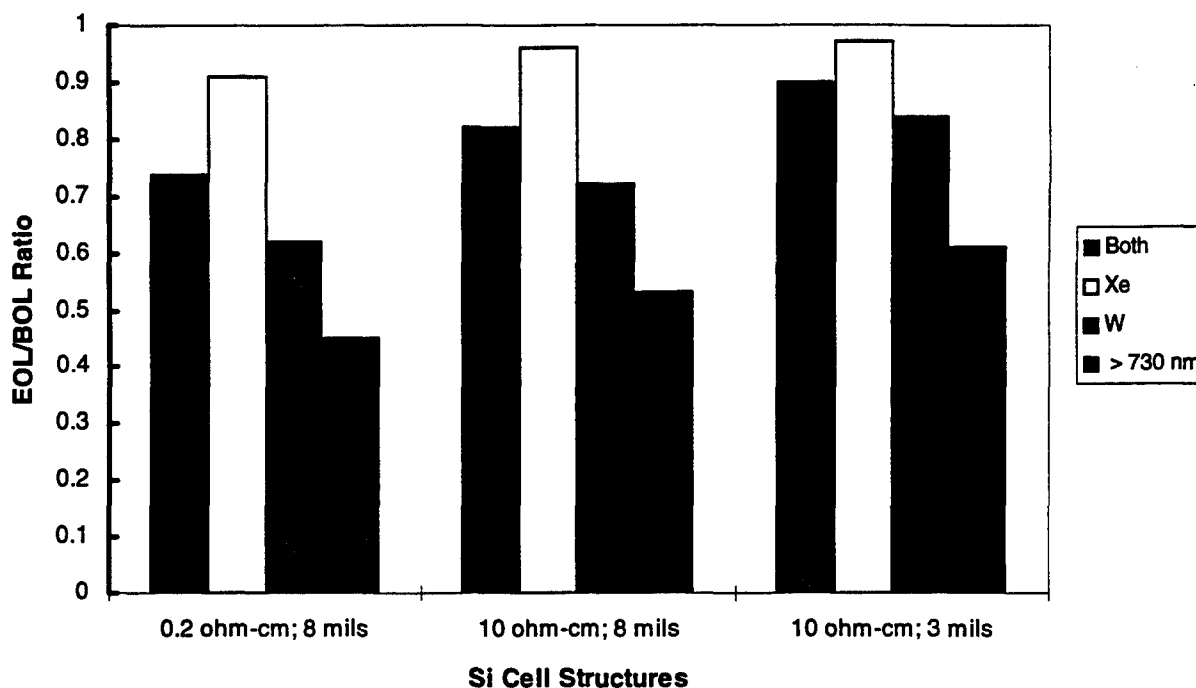
Figure 3.5. EOL/BOL ratios of data from Table 3.4. EOL/BOL ratio for $\lambda \geq 0.73$ μm has improved from 0.45 in first irradiation experiment to 0.61 with 10 ohm-cm, 75-μm-thick cell (3 mil cell).

Evaluation of the cells focused on the I-V characteristics measured before and after irradiation. ASEC's two simulators, the Hoffmann (two lamps) and an XT-10, complemented each other nicely for this task. The XT-10 provided illumination for most of the efficiency measurements, and the Hoffmann unit, coupled with AlGaAs filters, yielded the estimation of long-wavelength performance.

Based on the known spectral characteristics of the "red" filter on the Hoffmann unit and the known band gap of the AlGaAs filter, Mr. Iles, the ASEC Project Manager, has estimated that the currents measured under the AlGaAs should be about 0.75 of the current measured under the red filter only. However, measured ratios have been between 0.60 and 0.70 both before and after irradiation, suggesting that optical transmission losses are 5 to 15 percent between the AlGaAs filter and the cells. As a result, the currents we report in Table 3.5 may actually be understated by as much as 15 percent. But even with this additional current, the cells in this test failed to meet program requirements at long wavelengths.

Analysis of the data reveal several significant bits of information. First, the mean BOL efficiency excluding the controls is 13.2 percent, substantially less than the

18

Table 3.5. I-V Data For Si Solar Cells Having Different Thicknesses and Junction Depths.

Cell No.	Xenon-Lamp Simulator				Two-Source Simulator			Cell Thickness (mils)	Junction Depth (μm)
Cell Code: UU-Unirradiated, Unfiltered UF-Unirradiated, Filtered IU-Irradiated, Unfiltered IF-Irradiated, Filtered	V_{oc} (mV)	I_s (mA)	FF (%)	Eff. (%)	I_{sc} (mA) Both Lamps	+Red W (mA)	+Blue Xe (mA)		
3-UU	615	164.7	75.1	14.1	161.6	93.7	67.8	4.3	0.2
3-UF	577	58.0	76.4	4.7	59.2				
3-IU	503	139.9	70.8	9.2	138.4	73.2	65.6		
17-UU	620	161.3	74.7	14.3	162.6	94.9	67.7	4.1	0.2
17-UF	584	58.8	75.3	4.8	56.7				
17-IU	510	140.1	69.4	9.2	138.2	73.3	65.0		
17-IF					43.2				
207-UU	604	143.3	74.9	12.0	139.3	89.1	50.1	4.1	0.7
207-UF	573	59.5	73.8	4.7	52.5				
207-IU	506	118.3	74.8	8.3	117.9	70.1	48.0		
216-UU	581	133.2	74.5	10.7	129.6	83.0	46.2	4.2	0.7
216-UF	546	57.3	76.3	4.0	47.2				
216-IU	506	112.2	74.8	7.9	111.8	67.0	44.7		

Table 3.5. I-V Data For Si Solar Cells Having Different Thicknesses and Junction Depths (Continued).

Cell No. / Cell Code: UU-Unirradiated, Unfiltered; UF-Unirradiated, Filtered; IU-Irradiated, Unfiltered; IF-Irradiated, Filtered	Xenon-Lamp Simulator				Two-Source Simulator			Cell Thickness (mils)	Junction Depth (µm)
	V_{oc} (mV)	I_s (mA)	FF (%)	Eff. (%)	I_{sc} (mA) Both Lamps	+Red W (mA)	+Blue Xe (mA)		
313-UU	618	167.8	74.3	14.2	163.6	94.4	68.7	4.1	0.25
313-UF	576	58.5	75.0	4.7	58.6				
313-IU	514	146.2	75.7	10.5	140.9	74.5	66.2		
313-IF					43.9				
316-UU	623	170.0	74.5	14.6	165.4	96.5	69.2	4.2	0.25
316-UF	586	61.7	74.1	5.1	61.3				
316-IU	514	147.7	66.5	9.3	141.1	74.7	66.2		
27-UU	613	154.1	75.0	13.1	152.0	85.8	66.2	2.2	0.20
27-UF	574	56.4	75.2	4.5	52.0				
27-IU	525	151.5	75.1	11.0	141.5	76.8	64.7		
225-UU	603	132.7	75.9	11.2	132.4	81.4	51.0	2.3	0.7
225-UF	567	49.9	76.2	4.0	45.6				
225-IU	514	121.6	75.9	9.8	121.7	71.6	49.8		

Table 3.5. I-V Data For Si Solar Cells Having Different Thicknesses and Junction Depths (Continued).

Cell No. Cell Code: UU-Unirradiated, Unfiltered UF-Unirradiated, Filtered IU-Irradiated, Unfiltered IF-Irradiated, Filtered	Xenon-Lamp Simulator				Two-Source Simulator			Cell Thickness (mils)	Junction Depth (µm)
	V_{oc} (mV)	I_s (mA)	FF (%)	Eff. (%)	I_{sc} (mA) Both Lamps	+Red W (mA)	+Blue Xe (mA)		
43-UU	621	156.5	76.2	13.7	154.7	88.4	66.7	2.3	0.2
43-UF	583	53.5	76.1	4.4	54.3				
43-IU	519	144.5	76.1	10.6	140.4	75.9	64.7		
43-IF					50.3				
230-UU	600	132.5	68.7	10.0	130.2	82.5	48.2	2.1	0.7
230-UF	506	52.7	72.4	4.0	50.2				
230-IU	515	118.7	67.7	7.6	119.6	72.6	46.8		
324-UU	607	161.6	73.7	13.4	157.9	90.2	68.0	2.5	0.25
324-UF	563	55.2	74.4	4.3	53.5				
324-IU	517	147.6	73.6	10.4	143.7	77.1	66.3		
324-IF					45.2				
325-UU	578	154.6	75.6	12.5				2.4	0.25
325-UF	540	50.0	74.9	3.7					
325-IU	518	145.5	75.7	10.5	141.7	75.8	65.6		

Table 3.5. I-V Data For Si Solar Cells Having Different Thicknesses and Junction Depths (Continued).

Cell No. Cell Code: UU-Unirradiated, Unfiltered UF-Unirradiated, Filtered IU-Irradiated, Unfiltered IF-Irradiated, Filtered	Xenon-Lamp Simulator				Two-Source Simulator			Cell Thickness (mils)	Junction Depth (µm)
	V_{oc} (mV)	I_s (mA)	FF (%)	Eff. (%)	I_{sc} (mA) Both Lamps	+Red W (mA)	+Blue Xe (mA)		
14-UU (Thick Cell)	648	174.4	73.2	15.3	171.5	98.6	73.7	11.6	0.2
14-UF	614	63.0	72.1	5.2	62.0				
14-IU	573	124.6	72.5	9.6	120.4	56.0	64.6		
14-IF					33.4				
22-UU (Thick Cell)	644	173.6	76.2	15.8	170.3	97.6	73.6	11.0	0.2
22-UF	613	59.3	76.4	5.1	58.0				
22-IU	576	128.0	75.3	10.3	125.6	57.8	66.0		
A-UU (Control Cell)					161.5	93.7	67.4	3.3	0.2
A-UF					58.1				
A-IU	514	152.1	75.7	10.9	140.1	74.9	65.2		
C1-UU (Control Cell)					153.1	89.5	64.1	3.3	0.2
C1-UF					53.5				
C1-IU	516	147.0	79.0	11.1	136.1	74.3	61.8		

Table 3.5. I-V Data For Si Solar Cells Having Different Thicknesses and Junction Depths (Continued).

Cell No.	Xenon-Lamp Simulator				Two-Source Simulator					
Cell Code: UU-Unirradiated, Unfiltered UF-Unirradiated, Filtered IU-Irradiated, Unfiltered IF-Irradiated, Filtered	V_{oc} (mV)	I_s (mA)	FF (%)	Eff. (%)	I_{sc} (mA) Both Lamps	+Red W (mA)	+Blue Xe (mA)	Cell Thick- ness (mils)	Junc- tion Depth (µm)
654-UU (Control Cell)					159.1	91.7	68.1	3.3	0.2
654-UF					54.8				
654-IU	515	147.2	71.3	10.0	139.8	74.7	65.6		
UM-UU (Control Cell)					159.1	91.4	68.0	3.3	0.2
UM-UF					54.1				
UM-IU	515	147.7	73.4	10.3	139.1	74.0	65.1		

23

needed 16 percent to meet stack BOL efficiency requirements. Under the AlGaAs filter, the mean efficiency is 4.5 percent, giving a ratio of 0.34 for filtered and unfiltered efficiency. Decreased current causes most of the efficiency loss, as expected. The average I_{sc} (filtered)/I_{sc} (unfiltered) is 0.37, the average V_{oc} (filtered)/V_{oc} (unfiltered) is 0.93, and the product of these two ratios is 0.34, implying that the fill factor ratio is close to unity.

The efficiency with and without the AlGaAs filter should ideally give a ratio closer to 0.5 (actually, about 0.485—0.5 for the current and 0.97 for the voltage). Therefore, voltage loss under the filter is about twice the expected value.

We remind the reader that most of the BOL efficiency and current data were presented earlier if Figure 3.1. As the cell thickness decreases from 11 to 2 mils, the efficiency drops from 15 to about 13 percent for junction depths of 0.2 µm. In performing a linear regression on these data, the correlation coefficient r is 0.87. The thinnest cells with the 0.7-µm-deep emitter have efficiencies of 10 to 11 percent and seem to show about the same rate of decrease with thickness (not enough data to be absolutely certain). The decreased efficiency comes directly, as the data show, from lower I_{sc} values as the cells become thinner. Hence, we restate the importance of the point made earlier that the processing for these cells must yield improved current collection. The data also suggest that the current decrease at about the same rate regardless of junction depth (for 0.2 and 0.7 µm).

Turning now to the EOL/BOL relationships, the worth of the Hoffmann simulator becomes especially apparent. The cells were illuminated by either the xenon (+Blue in Table 3.5) or tungsten (+Red in Table 3.5) lamps before and after irradiation. These measurements yielded an EOL/BOL ratio for current generated under each lamp. By looking at these ratios, shown in Figure 3.6, it is obvious that the +Red response decreases much faster, by a factor of 3, with increasing cell thickness than the +Blue response, and the correlation coefficients are about 0.98 for both sets of data. The decrease of both is completely insensitive to junction depth (for 0.2 and 0.7 µm)

Therefore, a major result of this experiment is that in the tandem structure being developed in this program, considering both the decreased BOL performance of the thinner cells and the smaller EOL/BOL ratios for the thicker cells, optimum Si cell thicknesses are between 2 and 4 mils. Cell parameters must then be rigorously optimized to produce the highest BOL efficiency possible.

For V_{oc}, the average EOL/BOL ratio in this test is 0.85 (see Figure 3.7). Since irradiation has little effect on the fill factor, the product of an EOL/BOL current ratio of 0.8 and the voltage ratio yield an efficiency ratio of 0.682. We believe that this is about the best that can be achieved with any of the cells tested in this program. This value is too low to meet the stack EOL/BOL efficiency ratio of 0.8. This means that the bottom-cell current must be increased (idea of larger area described earlier) so that the top cell limits the current at BOL.

24
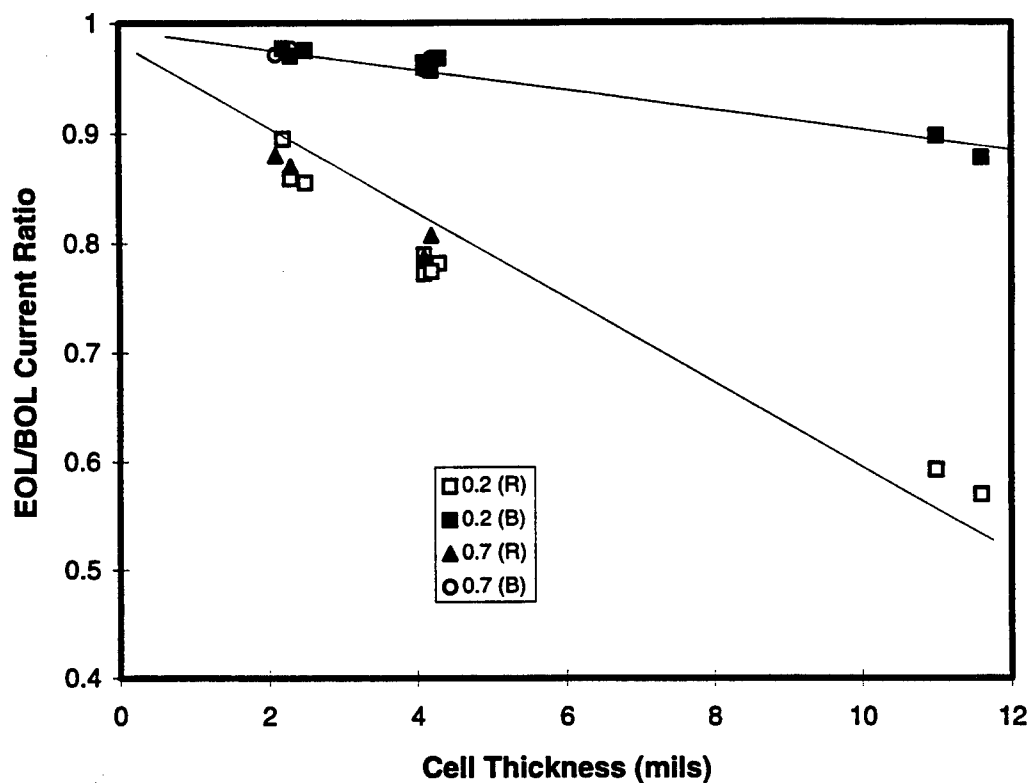
Figure 3.6. EOL/BOL current ratio for xenon (B) and tungsten (R) lamp illumination by Hoffmann simulator. Long-wavelength response decreases three times faster than short-wavelength response as a function of cell thickness.
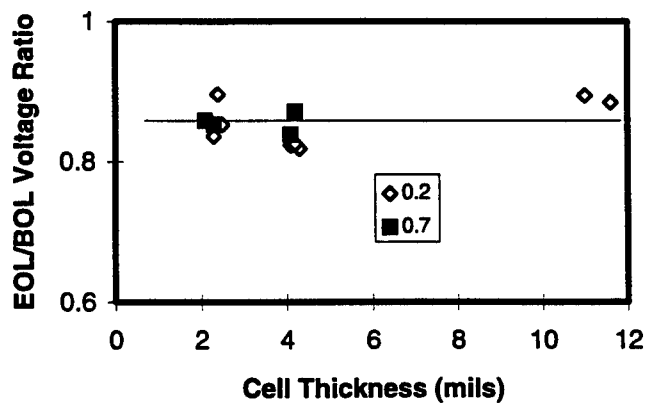
Figure 3.7. Illustration of voltage insensitivity to cell thickness.

3.5   Summary of Si Cell Development

The Si cells fabricated in the early part of this program using some modification of ASEC's standard production design are very good Si devices. Efficiencies ranged between 16 and 17 percent under AM0 illumination. These cells proved to be very "soft" to radiation damage in the long-wavelength spectral region that would be incident upon them in a tandem stack with a 1.7-eV top cell. These cell are relatively thick, about 200 μm (8 mils), and are made from low-resistivity (0.2 ohm-cm) Si slices. The EOL/BOL ratio for cell current is 0.45 in the spectral range of interest.

Improved devices were made using thinner Si slices of high-resistivity (10 ohm-cm) material, and the optimum thickness for the Si cell in the tandem stack is between 50 and 100 μm (2 and 4 mils). BOL efficiency decreases as cells are made thinner while the EOL/BOL ratio improves. EOL/BOL ratios greater than 0.6 were achieved for the relevant wavelength range, more than a 30 percent improvement above the original measurements.

Even with improved structures, the radiation performance of Si in the mechanical stack has been estimated to approach but fall short of that needed to meet the goals of the program's EOL/BOL ratio. There is a trade-off between BOL performance and EOL/BOL that must be taken into account when designing a cell such as the one being developed here. The cell design needs to address the application, particularly in the case when the two cells in a stack, monolithic or mechanically connected, degrade at different rates.

Plans for the development of a Si cell that incorporates some of the most advanced recent technologies were not implemented because of the program's early termination.

4.0   AlGaAs AND GaInAsP HIGH-BAND-GAP JUNCTIONS

4.1   Introduction

Preliminary modeling showed that the top cell to be stacked upon the Si bottom cell needs a band gap of about 1.70 eV. This band gap allows the currents in the cells to match at BOL, a requirement for series-connected tandem stacks and high BOL efficiency. Several of the III-V alloys have this band gap. For this program, two of them, $Al_{0.2}Ga_{0.8}As$ and $Ga_{0.7}In_{0.3}As_{0.4}P_{0.6}$, were likely candidates. Each has advantages and disadvantages.

The Al-Ga-As materials system, which includes GaAs, is the most mature of any III-V system. Other technologies, for example, light-emitting diodes and microwave transistors, are made mainly from GaAs and AlGaAs and have helped support development costs of the system. For solar cells grown by OMVPE, though, AlGaAs requires high growth temperatures, in the range of 750 to 800°C, to achieve long minority-carrier lifetimes. Growth temperature has been a major impediment to good quality AlGaAs/GaAs monolithic tandems (because high temperatures severely degrade tunnel junctions that are used to connect the GaAs and AlGaAs cells). Oxygen-related defects dramatically shorten minority-carrier lifetimes and, therefore, current collection, when growth temperatures are lowered. These are Al-related effects, i.e. they become more problematic as the Al concentration increases in AlGaAs. AlGaAs is also notorious for its DX center, a defect that traps majority electron carriers and makes high n-type doping of alloys difficult to achieve. Finally, the strength of the Al-C chemical bond makes carbon incorporation in AlGaAs almost a certainty, implying that n-type doping must also overcome a residual carbon background (or the layers will convert to p-type material).

AlGaAs also has attractive features. All the alloys are closely lattice-matched to the GaAs and Ge substrates that were planned for this program. The Al and Ga sources, TMA (trimethylaluminum) and TMG (trimethylgallium), are the cheapest and, related to the OMVPE growth, decompose at approximately the same temperature. This latter characteristic facilitates growing uniform compositions over large areas, which would be a major consideration for manufacturing because of its considerable impact on yield. Cost of source materials clearly is an obvious manufacturing issue. Finally, the chemistry of the Al-Ga-As system is well defined, and it is possible to etch these materials selectively to produce sophisticated structures or, to meet the needs of this program, to remove substrates from epitaxial layers.

The Ga-In-As-P system provides a non-Al option. Band gaps is this system range from GaAs (1.43 eV) to $Ga_{0.5}In_{0.5}P$ (1.9 eV) when alloys match the lattice constant of GaAs or Ge. At the program's beginning, only a handful of papers had been published about GaInAsP alloys that lattice-match GaAs (or Ge) although there is an extensive literature about alloys lattice-matched to InP because of the fiber optics in-

dustry. RTI had previous experience (NREL-funded work) with GaInAsP alloys with band gaps of 1.55 eV grown on Ge. So, extending this work to 1.70-eV band gaps was a logical extension to circumvent the Al problems of AlGaAs alloys. The alloy of interest for this program is $Ga_{0.7}In_{0.3}As_{0.4}P_{0.6}$, which has the desired band gap.

During the program, RTI's progress with GaInAsP and AlGaAs was matched and surpassed by the $Ga_{0.5}In_{0.5}P/GaAs$ monolithic tandem. The progress of GaInP, a material related to GaInAsP, supported the notion that GaInAsP is an alternative to AlGaAs. We believe that these quaternary alloys have the potential to be superior materials for space photovoltaics. Our early results with the GaInAsP and Yamaguchi's recent analysis [4] lend further credibility to this idea from our original proposal.

The major disadvantage of GaInAsP is the requirement to control the ratio of two Group III elements (Ga and In) and two Group V elements (As and P) simultaneously. There is only one alloy composition of this quaternary material that lattice-matches GaAs and provides the needed band gap concurrently, and if the ratios of the components change, compositional variation must accompany the changes. Controlling these ratios is difficult because the elements in each group have significantly different vapor pressures and because the thermal decomposition characteristics of the OMVPE sources, TMG and EDMIn (ethyldimethyindium), and the hydride gases AsH_3 and PH_3, the As and P sources, respectively, are not nearly as similar as TMG and TMA. The result can be variations in composition that affect both the band gap of the cell and the lattice match with the substrate. These, in turn, affect current matching between cells, which depends upon band gap, and the quality of the epitaxial growth, which requires close lattice matching.

To summarize this discussion, we were faced with two potential top-cell materials, each with advantages and disadvantages. At the beginning of the program, we did not have *a priori* reasons to choose one over the other. During the program, in spite of promising data from $Ga_{0.7}In_{0.3}As_{0.4}P_{0.6}$, the weight of the ease of lattice-matched growth, cost, and manufacturing factors led us to select $Al_{0.2}Ga_{0.8}As$ for the top-cell material. This, unfortunately, may have been a poor choice since we encountered considerable problems getting $Al_{0.2}Ga_{0.8}As$ cells, particularly n/p cells, to meet program goals.

The sections that follow contain details of the AlGaAs and GaInAsP cell growth, development, and testing.

4.2 AlGaAs Cell Development

4.2.1 AlGaAs Growth and Materials Characterization

Toward the end of the program's Phase 2 funding limitations forced the effort to be descoped. The work described in this section was completed prior to descoping. In Section 4.2.2 the descoped effort with a TMA source, purified by an improved method,

is described. This section focuses on the problems that were encountered during the AlGaAs growth, and the next on promising results that suggest solutions to these problems.

All the AlGaAs layers grown during this program were produced by OMVPE. The sources are TMG, TMA, AsH$_3$, DEZ, hydrogen selenide, and silane. SiH$_4$ and H$_2$Se are n-type dopants, delivered as dilute gases in hydrogen with concentrations of about 50 parts per million. Diethylzinc, an organometallic liquid, is the p-type dopant, and TMG, TMA and AsH$_3$ are the Ga, Al, and As sources, respectively. The reactor used for AlGaAs growth operates at reduced pressure, and most AlGaAs layers were grown at about 100 mTorr. This reactor also has a load-lock to prevent the inside of the growth tube from being exposed to the atmosphere. We believe that this type of system is essential for reproducible growth of high-quality AlGaAs layers. A point-of-use scrubber is used to remove residual oxygen and water vapor from the AsH$_3$, which is supplied as boil-off from a liquid source. Palladium-purified H$_2$ is the carrier gas and also has its own point-of-use scrubber to remove oxygen and water vapor. The key is to keep residual and background oxygen and water vapor level as low as is absolutely possible in the growth environment.

Aware of the difficulty growing AlGaAs alloys, particularly at low temperature, the first step in the program was to quantify the quality of RTI's material using the technique of DLTS (deep-level transient spectroscopy). Deep levels generally act as majority- and/or minority-carrier traps that will lower lifetimes, thereby limiting diffusion length and current collection. DLTS coupled with TPL (transient photoluminescence) and Hall-effect measurements of majority-carrier properties, provide a relatively good overall picture of the photovoltaic potential of AlGaAs or any other material.

A series of simple p/n junctions were fabricated to serve as DLTS samples. The samples have compositions of GaAs, Al$_{0.1}$Ga$_{0.9}$As, Al$_{0.2}$Ga$_{0.8}$As, and Al$_{0.3}$Ga$_{0.7}$As, and one of each was grown at temperatures of 660, 720, and 780°C. These samples were evaluated by Dr. R.K. Ahrenkiel of NREL (National Renewable Energy Laboratory), Golden, CO. The data from Dr. Ahrenkiel's testing of the GaAs and AlGaAs junctions are presented in Table 4.1.

The data of Table 4.1 essentially reinforce what is known about AlGaAs. Traps begin to appear at very low Al concentrations when growth temperatures are low. At any growth temperature, the trap content increases with Al content. This feature of these and other data strongly suggest that the entity responsible for trap formation is linked to the Al. Our belief at RTI is that a likely candidate for this observation is residual contamination of the TMA sources. For a single alloy composition, the trap density generally decreases with increasing growth temperature (except sample 1-1368, which behaved somewhat anomolously). Remarkably, even at a nominal growth temperature of 780°C, the trap density is about the same as the doping level in the base. This is likely a reflection of this particular TMA source as much as anything else.

These devices that Dr. Ahrenkiel examined have p/n polarities. The above data indicate one of the problems of the opposite polarity. If n-type AlGaAs were to be used

29

in the emitter and window layer, achieving high majority-carrier densities is problematic because of majority-carrier traps such as the ones identified in Dr. Ahrenkiel's data. Identification of trap-producing entities was not attempted because to do so was beyond the performance and funding scope of this contract.

Table 4.1. DLTS Analysis of GaAs and $Al_xGa_{(1-x)}As$ Junctions Grown at Temperatures of 660, 720, and 780°C.

AlGaAs Composition	Growth Temperature		
	660°C	720°C	780°C
x = 0.0	ND (1-1365)	ND (1-1376)	ND (1-1384)
x = 0.1	461 meV; 7.2e14 cm³ (1-1366)	ND (1-1381)	ND (1-1385)
x = 0.2	238 meV; 6.4e14 cm³ 488 meV; 3.4e15 cm³ (1-1367)	446 meV; 2.1e15 cm³ (1-1382)	467 meV; 1.4e15 cm² (1-1386)
x = 0.3	426 meV; 4.0e16 cm³ (1-1368)	383 meV; 5.5e16 cm³ 518 meV; 5.7e16 cm³ (1-1383)	354 meV; 4.8e16 cm³ 588 meV; 3.8e16 cm² (1-1387)

Notes:
1. ND signifies "none detected".
2. Trap energies are measured from the bottom of conduction band.
3. All traps are majority-carrier electron traps in cell base layers.

The minority-carrier properties, i.e. the minority-carrier lifetime, were estimated from TPL data for double-heterojunction structures for which an active AlGaAs (or GaAs) layer is "sandwiched" between two, thin AlGaAs window layers. These lifetimes, also measured at NREL by Dr. Ahrenkiel, ranged from subnanosecond (0.3 to 0.4 ns) to about 3 ns and varied with laser intensity to as much as 6 or 7 ns. As the laser intensity increases, Schockley-Read-Hall-like traps (nonradiative in nature) saturate and lifetimes increase. This type of behavior gives strong evidence that minority-carrier traps are abundant in the AlGaAs as well as the majority-carrier traps identified by DLTS.

If we assume an average minority-carrier lifetime of about 1 ns and a mobility of 1000 cm²/V-s for $Al_{0.2}Ga_{0.8}As$, which is probably a conservative value, a diffusion length of about 1.6 μm can be estimated using the Einstein relationship to evaluate the diffusion coefficient D_n. Using the EBIC (electron beam induced current) mode of an SEM, a sample (#1-1347) was measured, and the estimated diffusion length that resulted is 1.4 μm. The good agreement with the calculated value suggests that the materials

30

properties are in the range of the assumptions. This is a "good news/bad news" situation. The "good news" is that we have a fairly good understanding of the AlGaAs material quality; the "bad news" is that the materials properties may preclude this AlGaAs from reaching the potential needed to meet the program's goals. While we had hoped to lower temperatures for AlGaAs growth, the material quality from early efforts in the program indicated otherwise. As a result, most of the work was done with AlGaAs cells that were grown at temperatures around 780 to 800°C. Obviously, it is desirable to have the diffusion lengths as long as possible to maximize current.

It should be made very clear, though, that AlGaAs quality can vary fairly significantly with different TMA sources. While the bottle of TMA that produced the data described above may not yield material that meets program goals, we have seen other sources that enable better characteristics. This variability is one of the most vexing problems related to AlGaAs growth. In Section 4.2.2, work with a much better TMA source is described that offers hope of better devices and lower growth temperatures.

The surface of sample #1-1347, used for EBIC analysis, was also examined with cathodoluminescence (CL). Using CL, areas that contain crystalline defects characterized by nonradiative carrier recombination will appear as dark regions in otherwise light backgrounds. Dislocations are common crystalline defects that produce this type of behavior, In sample #1-1347, the defect density was determined to be about 2×10^3 cm^{-3}, which is the same as the defect density as in the GaAs substrate. Hence, the crystalline quality of the AlGaAs appears good and not the lifetime-limiting factor. This again points to deep levels, caused by residual impurities, as the limit to long minority-carrier lifetimes in this AlGaAs.

The singularly most important ramification of the above data is that the growth temperatures must remain high if photovoltaic quality AlGaAs is to be produced. We at RTI believe very strongly that residual oxygen in TMA sources necessitates the high temperatures.

A subtle result of the high growth temperatures involves the use of Ge substrates. Ge was to serve as the growth substrate for the top cell as part of achieving low production costs. Ge wafers are less costly than GaAs and can be removed with plasma-assisted dry etching, a production-compatible process. In Figure 4.1, PL (photoluminescence) scans from three $Al_{0.2}Ga_{0.8}As$ layers are displayed. The scan marked "A" comes from AlGaAs grown on Ge at 780°C, "B" comes from AlGaAs grown on GaAs at 780°C, and "C" from AlGaAs grown on Ge at 700°C. The PL emission intensity of the AlGaAs grown on GaAs is about 10 greater than for AlGaAs grown on Ge at 700°C, and both are significantly more intense than the AlGaAs grown on Ge at 780°C. In addition, the AlGaAs grown at high temperature on Ge shows a significant amount of sub-band-gap luminescence that is absent in the other two scans. These emissions are likely the result of high concentrations of Ge in the AlGaAs and are a direct consequence of the high growth temperature.

Since PL intensity is qualitatively related to minority-carrier lifetime, these data suggest that there may be additional performance problems if the AlGaAs is grown on Ge

without a thick buffer layer to reduce Ge incorporation into epilayers. Buffer layers, 5 or more μm thick, are common in the growth of GaAs cells on Ge substrates in the production reactors at ASEC. Such buffer layers are not complicated, but they do, in effect, double the growth time needed for the top cell, and any additional time means additional cost.

The discussion pursued in this section makes an unambiguous point: AlGaAs is a most difficult material to grow well consistently. While the above discussion highlights the problems of growth, good cells were produced when high growth temperature and GaAs substrates were used. P-on-n cells met the Phase 1 efficiency requirement of 17 percent. Cells such as that, coupled with Si cells capable of 8 percent under thin $Al_{0.2}Ga_{0.8}As$ layers, potentially meet the BOL efficiency requirement of the program. So, the picture is certainly not as bleak as the above discussion might lead one to believe. The advantages of AlGaAs, described in the introduction to this section, are powerful, particularly the lattice-matching and developed chemistry. But because of the chemical reactivity of Al with elements such as oxygen and carbon, AlGaAs is likely to remain a demanding material if the growth technology is OMVPE.
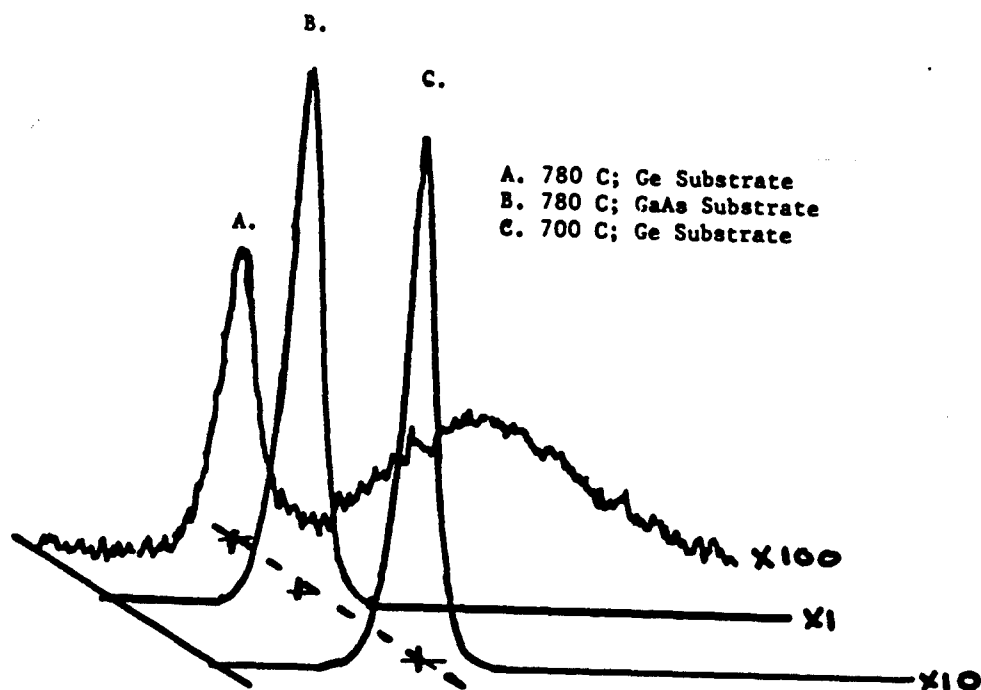

Figure 4.1. Photoluminescence spectra from three $Al_{0.2}Ga_{0.8}As$ layers grown at: (a) 780°C on Ge, (b) 780°C on GaAs, and (c) 700°C on Ge. Relative amplifier sensitivities are indicated for each scan.

4.2.2 Recent AlGaAs Developments Using Improved Al Sources

The results presented in the previous section describe growth difficulties that were encountered during Phases 1 and 2. The TMA sources used in that part of the effort were thought to be the best commercially available at that time. A new TMA source, purified in a proprietary manner (from EMF Limited, a U.K.-based company), became available at about the same time that funding limitations caused the main program effort to be descoped. As the last task of the program, a sample of this TMA was purchased and evaluated. The hope was that the quality of this TMA would be adequate to obviate many of the problems that were identified above.

The TMA did live up to its promised performance. In a side-by-side comparison with another source that was supposed to be "low-oxygen grade", the EMF material showed clear superiority. The TMA source was the only difference in these experiments.

The most logical parameter (related to solar cells) to evaluate this TMA is minority-carrier lifetime. Minority-carrier lifetime is the factor that determines the diffusion length when the carriers have reasonable mobility. Diffusion length, in large measure, controls the magnitude a cell's current, and low currents have been the pervasive problem for most of the AlGaAs cells fabricated during this program. To measure the lifetimes, we again relied on Dr. Ahrenkiel's facility at NREL. Samples were also sent to the Aerospace Corporation, but no data were returned. The samples consist of a double-heterojunction. The $Al_xGa_{(1-x)}As$ active layers are all about 5 μm, and the Al fraction x has nominal values of 0.1, 0.2, and 0.3. In each sample the active layer lies between two $Al_{0.8}Ga_{0.2}As$ window layers that are about 0.1 μm, and a thin GaAs cap layer, added to facilitate contacting samples for Hall measurements, was grown on the top window layer. This GaAs layer was removed by selective etching for PL and TPL measurements. Growth temperatures were 620, 680, 720, and 780°C. All samples were grown on semi-insulating GaAs substrates so that Hall measurements could be made.

It is worth making the point again that the only difference between the two sets of samples that were prepared is the TMA source. Both TMA sources were connected to the OMVPE system, there were no system changes made during the growths, and the system was meticulously checked for leaks with a helium leak detector prior to initiating sample growth. The samples grown with the EMF TMA were grown after the set that used the "zero-oxygen" grade of TMA; so, had a leak developed during the growth, the oxygen would have affected either both sets of samples or only the set using the improved TMA.

Prior to sending the samples to NREL, room-temperature PL measurements were made. By accounting for differences in laser power and detector sensitivity and correcting for carrier concentration differences (carrier concentration from Hall data), the relative emission intensities were qualitatively estimated. These data are presented in Figure 4.2.
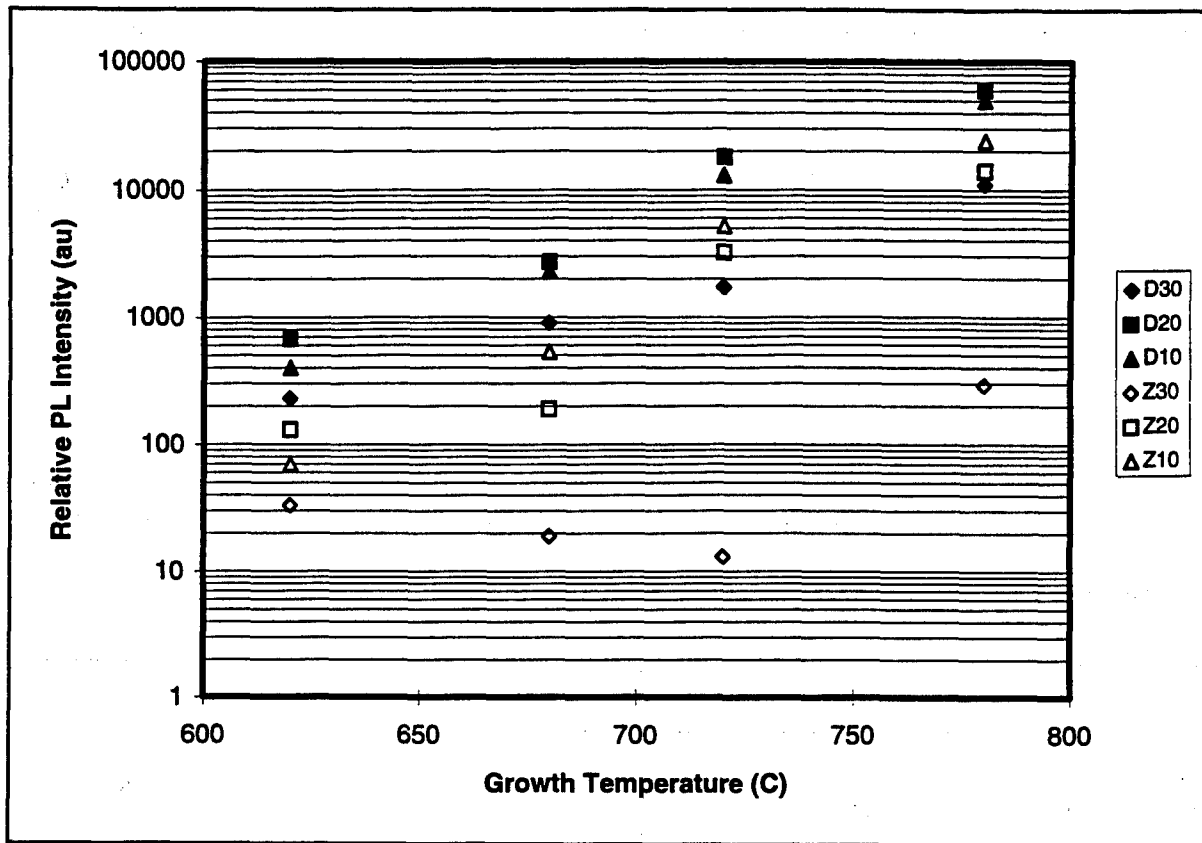
Figure 4.2. Relative PL intensity from AlGaAs samples grown with improved TMA source (solid characters marked D10, D20, and D30, where numeral indicates Al fraction x) and commercially available zero-grade oxygen source (open characters marked Z10, Z20, and Z30).

The data in Figure 4.2 show several trends. First, for any AlGaAs composition, the PL intensity decreases about one decade per 100 C° drop in growth temperature, a behavior that is not unexpected. Only the samples marked Z30 ($Al_{0.30}Ga_{0.70}As$ grown with "zero-oxygen" TMA) show erratic behavior. Second, and more importantly, all of the samples grown with the improved TMA (solid symbols) have greater PL intensity than the respective sample grown with the other source (open symbols). This indicates that the minority-carrier lifetime is qualitatively longer in the more luminescent samples and that this improved source does produce better quality AlGaAs.

The lifetime data from NREL for these same samples give a semi-quantitative perspective but confirm qualitative trends indicated in Figure 4.2. The NREL data are presented in Table 4.2.

Table 4.2. Transient Photoluminescence Decay of AlGaAs Double-Heterojunction Structures Grown with Two Aluminum Sources.

Growth Temp. (°C)	TPL Decay Time (ns)					
	$Al_{0.1}Ga_{0.9}As$		$Al_{0.2}Ga_{0.8}As$		$Al_{0.3}Ga_{0.7}As$	
	D	Z	D	Z	D	Z
620	0.16	0.16	0.2	0.18	0.15	0.14
680	0.73	0.42	1.1	0.19	0.43	0.14
720	6.2	1.0	7.8	0.66	3.1	0.16
780	21.3	5.9	18.3	1.9	2.3	0.18

Notes: System response time about 0.14 ns. Data not corrected for interface recombination velocities. D source from EMF, Ltd. Z source is "zero-oxygen" source. All samples illuminated with equal laser powers.

The data of Table 4.2 show two general regimes. The higher temperature regime ($\geq 720°C$) has the D samples with markedly longer lifetimes by factors that range from about 2.6 to more 10. The samples grown at 680 and 620°C comprise the second regime. Here the lifetimes of alloys grown with the two TMA sources are about the same or vary by no more than a factor of 3. For all the samples grown at 620°C, lifetimes are close to system response, meaning that the actual lifetimes may be shorter.

These data have a very logical explanation. At high temperatures we are clearly seeing the effects of reduced minority lifetime "killers" in the D samples grown with the improved TMA. Since the TMA is the only known difference in the growth, it likely accounts for the lifetime differences. At lower temperatures, we may be seeing the effects of residual oxygen contamination from other sources such as the TMG that combine more effectively with TMA as the growth temperature decreases.

The presence of some traps even in the material grown at higher temperatures is suggested by varying the laser power. As the power increases, the additional generated carriers occupy trap site. As more and more of the traps are occupied, the material begins to act as if the traps were absent, and lifetime of excess carriers increases. This behavior has been observed in almost all of the samples prepared for this experiment. An example is found in Figure 4.3 that shows the data for the $Al_{0.3}Ga_{0.7}As$ grown at 720°C with the D source. As laser power increases from 0.1 to 16 mW, the lifetime

35

varies from 3.1 to 25.0 ns, going through a peak at 30 ns and then decreasing slightly to 25 ns.
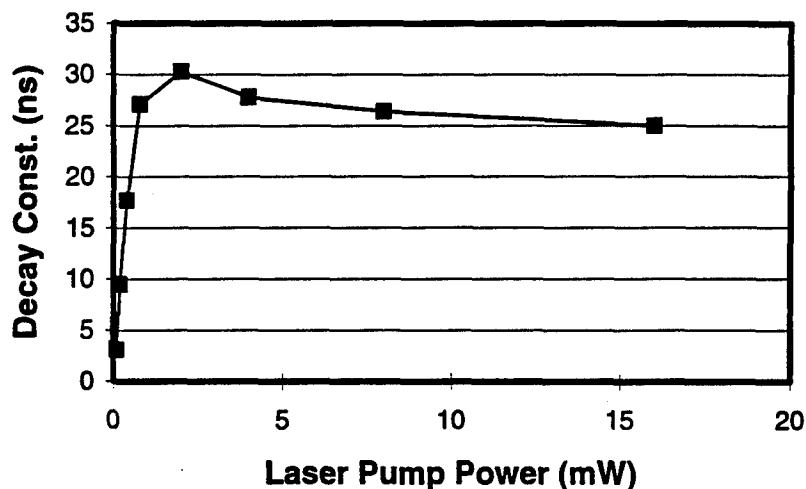
Figure 4.3. Effect of increasing laser pump power on TPL decay constant. This behavior suggests the presence of Shockley-Read-Hall-like recombination centers. Saturation of these centers allows minority-carrier lifetimes to lengthen and enables radiative recombination to place the upper limit on measured values.

Since the saturation effect occurs at relatively low laser powers when small numbers of excess minority carriers are generated, we assume that the trap density also is small. This may be added evidence that the material quality is good. We do not have an explanation for the decrease in decay constant at the higher laser powers. The radiative lifetime is the longest that should be seen in direct band-gap materials such as $Al_{0.2}Ga_{0.8}As$. If we assume that the radiative recombination coefficient B of $Al_{0.2}Ga_{0.8}As$ is similar to GaAs (about 2×10^{-10} cm^3 sec^{-1}) and electron carrier concentration $n \sim 10^{17}$ cm^{-3} in the layers, the inverse product of these two parameters gives the approximate radiative lifetime, in this case, about 50 ns. So, the data in Figure 4.3 suggest that the sample has sufficient quality for the radiative limit to be approached with relatively modest laser pump power.

Based strictly on the lifetime criterion, the AlGaAs grown at 720°C with the new source should perform at least as well as AlGaAs grown at 780°C earlier in the program with "less clean" sources, and growth at 780° should produce superior cells to those fabricated earlier.

This last point, growth and fabrication of better AlGaAs cells, needs to be proven experimentally but does depend on the total quality of every component in the growth environment, including the carrier gas and dopant gases, TMG, and As source. Per-

formance also depends on substrate quality and pregrowth preparation. And finally, it depends on all parts of the structures functioning as designed.

At the very least, this improved TMA source seems to offer the possibility that AlGaAs can meet the goals of this program technically. Cost, since the source is expensive, may be a different story. We attempted to grow a series of $Al_{0.2}Ga_{0.8}As$ cells with the improved TMA, but problems with the window layer and possibly the antireflective coating prevented these junctions from achieving the performance that was expected of them. These cells will be described in the next section along with the rest of the AlGaAs cell results.

4.2.3 AlGaAs Cells and Cell Testing

Without question, the most frustrating part of this program has been the performance of $Al_{0.2}Ga_{0.8}As$ junctions. The parameter, as indicated in the discussions of the preceding sections, that has been the most problematic is the cell current, and the problem seems to be worse for n/p $Al_{0.2}Ga_{0.8}As$ cells. This problem consumed an inordinate amount of contract resources, much more than was planned. At the program's inception, RTI was growing p/n cells, both AlGaAs and GaInAsP. Because ASEC produces n/p Si cells, both $Al_{0.2}Ga_{0.8}As$ cell polarities were modeled using the code PC-1D. We believe that PC-1D has reasonably accurate materials parameters for $Al_{0.2}Ga_{0.8}As$, and materials parameters are an essential part of any device simulation.

To make the simulations as relevant as possible to the experimental observations to that point in the program, several of the code's parameters were changed. The carrier lifetimes were shortened, and interface recombination velocities (at the surface and between emitter and window layers) were made fairly high. Our belief was that this defined a conservative set of parameters that should understate $Al_{0.2}Ga_{0.8}As$ cell potential. But the simulation produced numbers that were very similar to those seen experimentally for the p/n cells, having currents only slightly larger than experimental ones. The simulation further indicated that the currents of the n/p cells should be larger than for the p/n cells. However, experimentally the n/p $Al_{0.2}Ga_{0.8}As$ currents are about 20 percent lower. The results are summarized in Table 4.3. Note that the current densities shown in Table 4.3 are 22-24 mA/cm^2, which has been the program's goal for the stacked structure.

Table 4.3. Simulated Performance of N-P and P-N $Al_{0.2}Ga_{0.8}As$ Solar Cells.

Cell Type	V_{oc} (mV)	I_{sc} (mA)	FF (%)	Eff. (%)
N-P	1.168	95.89	79.2	16.4
P-N	1.185	92.29	80.5	16.3

Fairly early in the program, the Phase 1 performance goal was met using a small-area p/n $Al_{0.2}Ga_{0.8}As$ cell. The active-area of the device is 0.136 cm^2 and the I-V curve for the sample (#1-1601) is shown in Figure 4.4. The cell was measured at ASEC using a two-source simulator. Although this cell is a small-area device, it nonetheless demonstrates that $Al_{0.2}Ga_{0.8}As$ can meet needed performance, and producing larger cells is usually a matter of optimizing growth and processing. These optimizations were under way when the decision to use n/p Si cell was made. This decision forced the same polarity on the top cell since the structure is a two-terminal, series-connected device. At that point, we abandoned the p/n $Al_{0.2}Ga_{0.8}As$ effort.
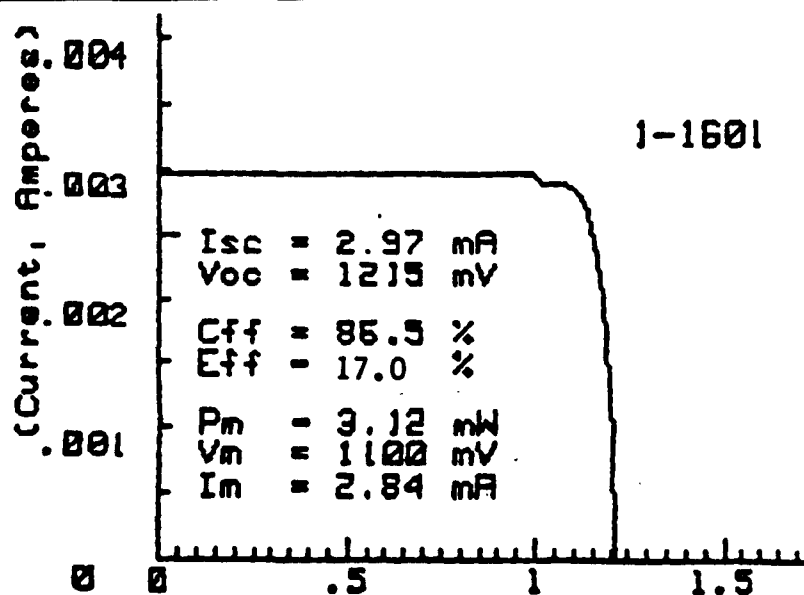
Figure 4.4. I-V characteristic of $Al_{0.2}Ga_{0.8}As$ solar cell (#1-1601). The device active area is 0.136 cm^2, giving a current density of 21.8 mA/cm^2. Device measured under a two-source simulator.

Work with the n/p $Al_{0.2}Ga_{0.8}As$ cells began strongly. Several 2 x 2 cm^2 cells were fabricated. These cells have thin emitters that are about 0.05 μm thick. The best of these devices showed a V_{oc} of 1.22 V and an I_{sc} of 61 mA before an AR coating was added. This current projects to 81.7 mA, or 20.4 mA/cm^2 (total area), with the AR gain that we normally see for these devices. Unfortunately, the fill factor was only 0.78. The fill factor would have limited cell efficiency to about 14 percent had the AR coating been added. Had the fill factor been the 0.865 of the best p/n cell, the efficiency projects to about 16 percent. Because electrons have much higher mobilities in GaAs and AlGaAs than holes, an emitter in an n/p cell can be much thinner than in a p/n cell without greatly increasing series resistance of the device. Mobilities in AlGaAs are lower than in GaAs, and apparently the very thin emitters do add to series resistance. We have measured mobilities of about 1500 cm^2/V-s for $Al_{0.2}Ga_{0.8}As$ doped at 8 x 10^{17} cm^{-3} (carrier concentration determined for thick $Al_{0.2}Ga_{0.8}As$ layers using same dopant flow

as cells; very thin layers, though, will usually have lower concentrations because the layer is grown so quickly that growth environment does not reach equilibrium). The result is that the emitter sheet resistance is well over 1000 Ω/sq. Electron mobility and the carrier concentrations in $Al_{0.8}Ga_{0.2}As$ windows are even lower. So, most of the majority-carrier conduction is confined to the thin emitter.

The next step was obviously to grow cells with thicker emitters. *This step initiated what we believe to be the central issue for the n/p $Al_{0.2}Ga_{0.8}As$ cells grown in this program: As the cell emitters were thickened, cell currents decreased. Spectral response data confirmed that the added loss comes in the short-wavelength portion of the spectrum.* In the next section on the development of GaInAsP cells, a comparison of spectral responses from an $Al_{0.2}Ga_{0.8}As$ cell and a GaInAsP cell are shown in Figure 4.9, and the difference in short-wavelength is glaring. GaInAsP cells met cell current expectations.

We did not solve this problem before the program was descoped and the effort terminated. Progress was made by optimizing growth conditions, doping concentrations, window layer composition, and layer thicknesses as much as possible. Typical cells had the following parameters: V_{oc}, J_{sc}, and FF were 1.18 V, 19 mA/cm^2, and 0.82, respectively. Efficiencies, with these and similar parameters, ranged between 13 and 15 percent. At the very, very best, these cells would have only marginally met the BOL efficiency requirement if stacked on an 8-percent Si cell with absolutely no interconnect losses and if the efficiencies of the AlGaAs cells did not degrade when substrates were removed. There was, in effect, no engineering margin for any parameter variation, a condition that would make attempts to manufacture such a device difficult, risky, and costly (low yield).

One approach that seemed to hold promise was a heterojunction cell. In a true heterojunction cell, the emitter and base are made of different material. The rationale for this type of cell in this program is straightforward. We replaced a very thin emitter with a layer, somewhat thicker, that served both as an emitter and a window. Since this layer could be made from a material with an indirect band gap, photon absorption would be limited, and the base would serve as an absorber layer.

This idea produced positive results for a structure that has a 3-μm-thick $Al_{0.2}Ga_{0.8}As$ base and about a 0.1-μm-thick $Al_{0.8}Ga_{0.2}As$ emitter. Small-area cells were produced, and the best of these has the following I-V characteristics: V_{oc} = 1.18 V, J_{sc} = 23.3 mA/cm^2 (active area; 22.1 mA/cm^2 with 5-percent grid obscuration), and FF = 0.81. The efficiency is 16.5 percent (15.7 percent with 5-percent grid obscuration). In concept, we have attempted to remove current generation in the emitter and force all generation to the base. The idea worked, and modest improvements in the voltage and fill factor would produce a 17-percent cell. We believe that this was the first report of a successful heterojunction cell.

A series of heterojunction cells was grown to identify important process and structure parameters. The I-V data for these 2 × 2 cells are shown in Table 4.4. These cells have grids that cover 9 percent of the surface; so, currents would be slightly higher

for 5- to 7-percent grids. Nonetheless, the current densities of these cells are very close to 20 mA/cm^2 for the best ones. Also, these samples were measured at RTI using a GaAs cell to set simulator intensity, and currents are slightly underestimated (by about 10 percent). These cells come very close to meeting projected performance. The parameters that were varied are emitter growth time and temperature and purge time between the base and emitter growths.

Table 4.4. I-V Data For 2 × 2 AlGaAs Heterojunction Cells.

Cell No.	Growth Temp. Of Base (°C)	V_{oc} (V)	I_{sc} (mA)	FF (%)
1-1858	780	1.06	68.0	75
1-1861	800	1.07	67.0	75
1-1862	800	1.16	38.0	76
1-1865	800	1.13	74.0	74
1-1868A	800	1.16	79.8	78
1-1868B	800	1.18	78.2	79
1-1869A	800	1.13	78.2	80
1-1869B	800	1.18	78.2	78
1-1872	800	1.17	73.1	82

Plans to improve the 2 × 2 heterojunction cells further had to be postponed because the intense, and unfortunately futile, effort to get higher currents in the $Al_{0.2}Ga_{0.8}As$ cells depleted contract financial resources. The effort expended on $Al_{0.2}Ga_{0.8}As$ was far greater than had been anticipated when planning the program.

The final attempt to produce high-quality $Al_{0.2}Ga_{0.8}As$ cells came during the descoped effort. Ten cells were to be grown. The cells were grown with a TMA source from EMF, Ltd., at a planned temperature of 780°C. We were trying to produce n/p cells with 0.25-μm-thick emitters and 2.5-μm-thick bases. Hall measurements performed on separately grown layers showed carrier concentrations of 9×10^{17} and 1×10^{17} cm^{-3}, respectively, for the emitter and base. A structure was grown and examined by SEM to verify that all component layers were in place. SEM did show that Se, the emitter dopant, diffused significantly at 780°C, and the junction depth is closer to 0.4 μm. A SEM cross-section of the $Al_{0.2}Ga_{0.8}As$ cell is shown in Figure 4.5 below.
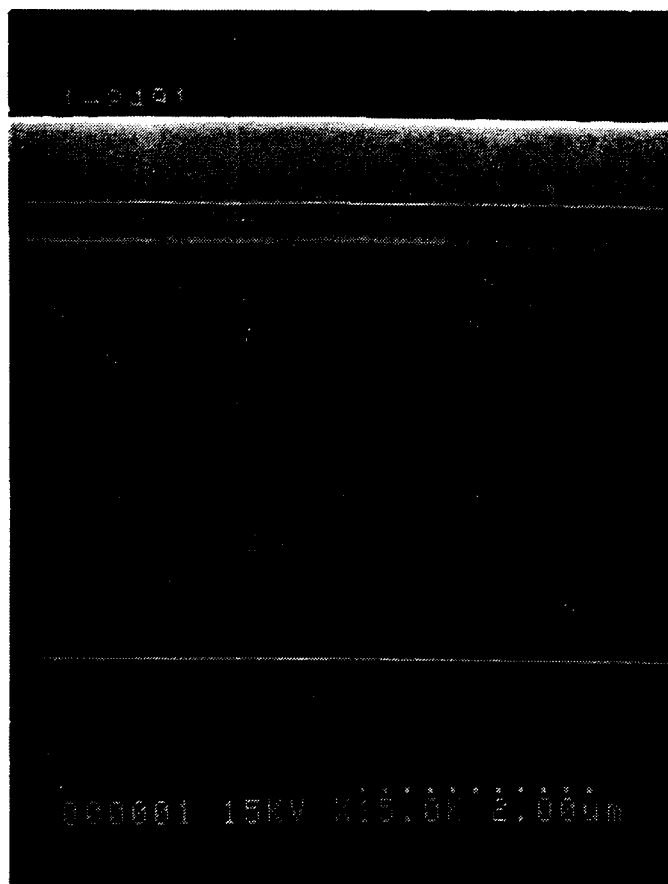
Figure 4.5. SEM cross-section of $Al_{0.2}Ga_{0.8}As$ solar cell. Sample grown at 780°C. Se diffusion from emitter causes deeper junction than planned.

To reduce Se diffusion, the growth temperature was lowered to 740°C, and a series of ten $Al_{0.2}Ga_{0.8}As$ cells were grown and processed through the application of a two-layer ZnS/MgF_2. Cells were evaluated under a xenon-lamp simulator at RTI using a GaAs cell to set simulator intensity. This GaAs cell was calibrated under ASEC's two source simulator using balloon-flown cells as the standards. Using a GaAs cell for the simulator reference underestimated the actual $Al_{0.2}Ga_{0.8}As$ currents by about 10 to 12 percent on our simulator (based on a comparison of cells measured under the RTI and ASEC simulators).

The I-V performance of these cells is very poor. But the problem appears to be structural, particularly the window layers, as much as anything.

Several cells, which originally had deep, bluish-blackish colors, began turning green. This means that either the $Al_{0.88}Ga_{0.12}As$ window (AlGaAs alloy composition kept this great to minimize photon absorption) is oxidizing, or ZnS is reacting chemically with the windows. During growth, if the alloy composition drifted to an Al fraction greater than $x \approx 0.9$, AlGaAs becomes hygroscopic (strong affinity for water vapor) in addition to being highly reactive with oxygen. And finally, the AR gain for all the cells was very poor, again suggesting something amiss with the surface structure. We have observed this type of behavior with other samples when the window layer was oxidized.

In the I-V characteristics of the cells, a blocking potential appears near the V_{oc} point for most of the samples, and this potential behaves as if a junction with p/n polarity is included in the structure. If such a junction exits, the p layer is almost certainly the window layer or the BSF layer, both of which are higher Al-composition AlGaAs than $Al_{0.2}Ga_{0.8}As$. The higher composition would be more difficult to dope n-type heavily and more easily converted to p-type materiel because of increased residual carbon incorporation (the Al-C chemical bond is very strong); since the BSF layer is already p-type, the evidence points to the window layer. The blocking potential lowers the fill factor and V_{oc} fairly dramatically.

Finally, most of the cells show an inordinate amount of shunting, which also degrades fill factors. Forward biasing two of these devices gave some insight into this problem. Rather than a uniform red emission, as would be expected for a defect-free device of this band gap, the cells show a dense number of bright red spots in an otherwise dark background. This means that most of the current is confined to these defects that act as device shunts. We do not know the origin of these shunts, but substrate defects, substrate preparation, particulate formation during growth, and other causes are possible sources.

There are no contract resources available to analyze these samples more rigorously. An impending laboratory shutdown and the lack of resources also prevented their regrowth before the program's conclusion.

It is our firm belief that these cells, whose I-V characteristics are given in Table 4.5, do not satisfy the objective of this experiment. The objective is to evaluate $Al_{0.2}Ga_{0.8}As$ cells grown with a hopefully superior TMA source. It is very likely that the structural problems encountered with these cells mask the quality, good or bad, of the source. We, therefore, draw no conclusions about the TMA source from these cells.

It is our intention to repeat the growth of these cells using IR&D funding. We expect improved performance and plan to replace these 10 cells with ones that, we hope, will reflect the material quality that we believe this TMA source capable of producing.

Table 4.5. I-V Characteristics of Final $Al_{0.2}Ga_{0.8}As$ Solar Cells Grown in Program's Descoped Effort to Evaluate New TMA Source.

Cell Number	V_{oc} (V)	I_{sc} (mA)	FF (%)
1-2491	1.091	31.3	78-80
1-2493	1.146	30.4	78-80
1-2494	1.151	32.3	75
1-2495	1.135	35.4	65
1-2497	1.008	41.9	60
1-2498	1.000	51.7	50
1-2499	1.020	53.5	60
1-2500	1.007	59.8	60
1-2501	1.014	47.4	60
1-2502	1.019	49.4	60

Note: Cells measured under xenon-lamp simulator using GaAs standard.

4.3 GaInAsP Cell Development

4.3.1 GaInAsP Cell Growth

Like the AlGaAs, GaInAsP alloys were grown by OMVPE. The reactor used for the growth has a vertical flow geometry with a flat, SiC-coated, graphite susceptor that sits perpendicular to the gas flow and operates at atmospheric pressure. The growth temperature for almost all of the GaInAsP layers remained constant at 675°C, fully 100 C° lower that those used for comparable AlGaAs alloys. The Ga, In, As, and P sources are TMG, EDMIn, AsH_3, and PH_3, respectively. Zn from a diethylzinc source and Se from a H_2Se source diluted with H_2 to about 50 parts per million were the p- and n-type dopants, respectively. Palladium-purified H_2 served as the carrier gas.

GaInAsP was grown on both GaAs and Ge substrates. For growth particularly on Ge, the nearness of the lattice match between an epilayer and substrate is extremely important. For this work, relatively thin Ge wafers were used to reduce the time required for substrate removal, which yields a thin top cell that is bonded to a Si bottom

cell. If epilayers are mismatched, the resulting strain bows the Ge wafer, making processing difficult, if not impossible, by contact lithography. The residual strain also makes the wafers exceedingly brittle, so much so in extreme cases of mismatch that they seem to explode if they fracture. A factor such as this will likely have a strong negative impact on manufacturability of devices and accentuates the need for very tight compositional control with this quaternary alloy.

In growing GaInAsP on Ge, we also observed some evidence of autodoping. Autodoping is the phenomenon of Ge atoms from the substrate being incorporated into the epitaxial layer. The source of Ge can be either solid state diffusion or vapor transported Ge from the backside of the substrate or the susceptor. The effect is demonstrated in Figures 4.6 and 4.7. These figures show electrochemical profiles of carrier concentration in GaInAsP layers that were grown on side-by-side GaAs and Ge wafers, respectively. The profile of the GaInAsP/GaAs structure is well-behaved and indicates a clear epilayer/substrate interface. The profile of the GaInAsP structure, however, indicates that As and/or P have diffused into the Ge, the elevated carrier concentration in the GaInAsP suggests Ge (an n-type dopant in this material) has been incorporated in the epilayer.

Diffusion into Ge is of little concern since the substrates are to be removed in the final structures. Incorporation of Ge into the base of an n/p GaInAsP cell is a concern if the Ge concentration exceeds the p-type base doping, producing an n/p/n structure. This second p/n junction, the lower one formed near the cell/substrate interface, will block current and produce an opposing photovoltage to the desired one. This effect was observed in some of the early GaInAsP cells grown on Ge although it was not verified if the second junction formed in the p-type Ge substrate or in a p-type GaAs buffer grown prior to the GaInAsP. In any event, had the GaInAsP cells been pursued, this potential problem would have required attention.

The material quality of the GaInAsP overall seemed quite good. Photoluminescence intensities from the layers were strong, suggesting good minority-carrier properties.

4.3.2 GaInAsP Cells and Cell Testing

When cells were fabricated, two sizes were fabricated. By using small-area cells, more test pieces could be fabricated from a single wafer. The small cells were processed with a concentrator mask and have active areas of 0.136 cm^2. Since the grid obscuration of this mask is greater than 15 percent, we report active-area currents or current densities for these cells. Large-cells, 4 cm^2, to meet the program requirements were also fabricated, and total-area currents (adjusted for a 7-percent grid) are reported for these devices.
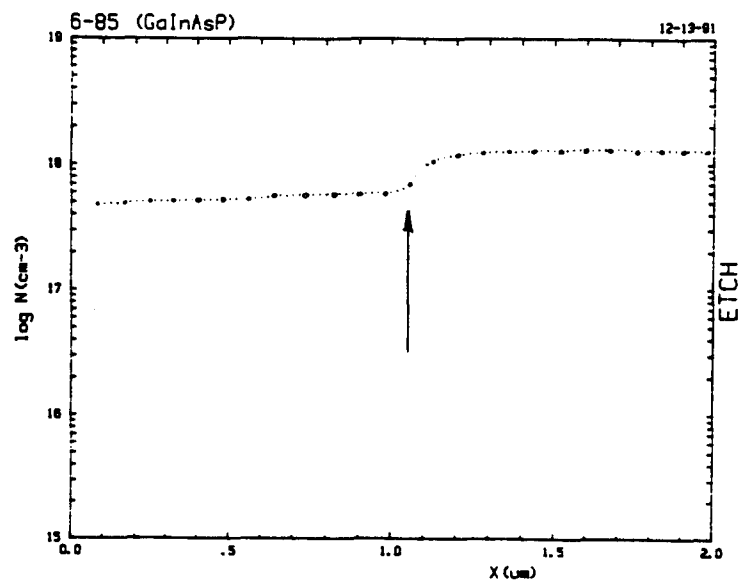
44

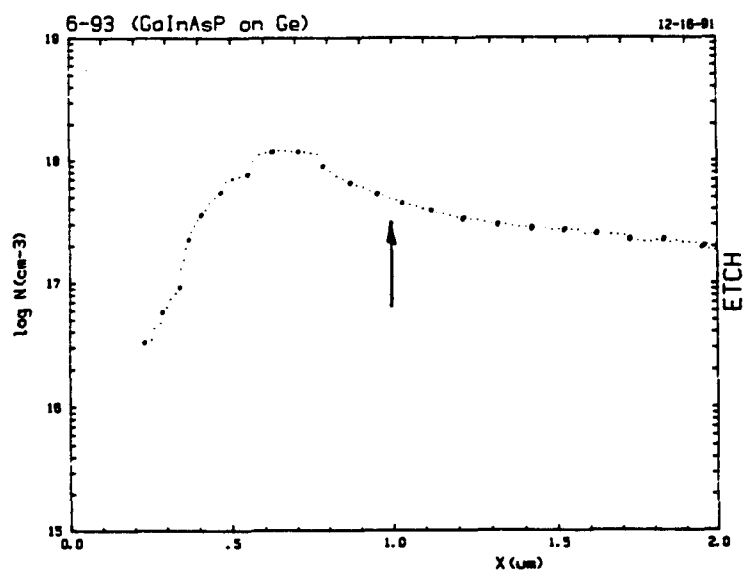**Figure 4.6.** Electrochemical profile of GaInAsP layer grown on GaAs substrate.

Figure 4.7. Electrochemical profile of GaInAsP layer grown on Ge substrate

45

Metallization for the GaInAsP devices was standard. For n-type material, layers of AuGe alloy (12 percent Ge), Ni, and Au formed the ohmic contact, and Ti/Au was used for p-type contacts.

Development of the GaInAsP devices proceeded rapidly early in the program. The results were very encouraging. In fact, the very first junction produced the following parameters: V_{oc} = 1.1 V; J_{sc} =18.1 mA/cm^2 (adjusted for 7 percent grid obscuration); and FF = 0.80. These parameters yield an efficiency of 11.8 percent and were measured under a two-source simulator (Hoffmann simulator) at ASEC. This simulator gives a more accurate AM0 representation than a single-source, xenon-lamp simulator such as the one in use at RTI. The cells used to set simulator intensity were calibrated in a JPL balloon flight. The structure of this first cell is shown in Figure 4.8 in schematic form. This cell structure is very conventional, and little attempt was made to produce optimized devices early in the program. At that point, we were more concerned with establishing baseline performance for the GaInAsP since this material had not been used for solar cells prior to this program.

This first structure has some weaknesses. First, the base layer is too thin for complete absorption of incoming photons with energies greater than the bandedge. Second, and more important, the window layer needed improvement to provide better minority-carrier confinement. The band gap of the GaInP is about 1.85 eV, or only 150 meV greater than the GaInAsP. The difference in band gap distributes between the conduction and valence bands in any heterojunction system. Therefore, in the case of these materials, the valence band offset, needed to confine hole minority carriers, will not see the full 150 meV. By changing the window material to $Al_{0.5}In_{0.5}P$, which lattice matches GaAs and has a band gap of about 2.4 eV, the offset in the valence band is significantly increased and minority-carrier confinement improved. The importance of the window layer is suggested by the data in Figure 4.9. Here the spectral responses of $Al_{0.5}In_{0.5}P$-windowed GaInAsP and $Al_{0.7}Ga_{0.3}As$-windowed $Al_{0.2}Ga_{0.8}As$ cells are compared. The short-wavelength response of the InGaAsP cell is clearly superior to that of the AlGaAs cell. In subsequent versions of GaInAsP cells the windows were changed to AlGaP. A p-type $Ga_{0.5}In_{0.5}P$ back-surface-field layer was tried to passivate the bottom of the GaInAsP base layer but was found to be relatively ineffective. We ascribe the ineffectiveness to most of the band-gap offset being in the valence band, thereby providing little containment of minority-carrier electrons by the conduction band.
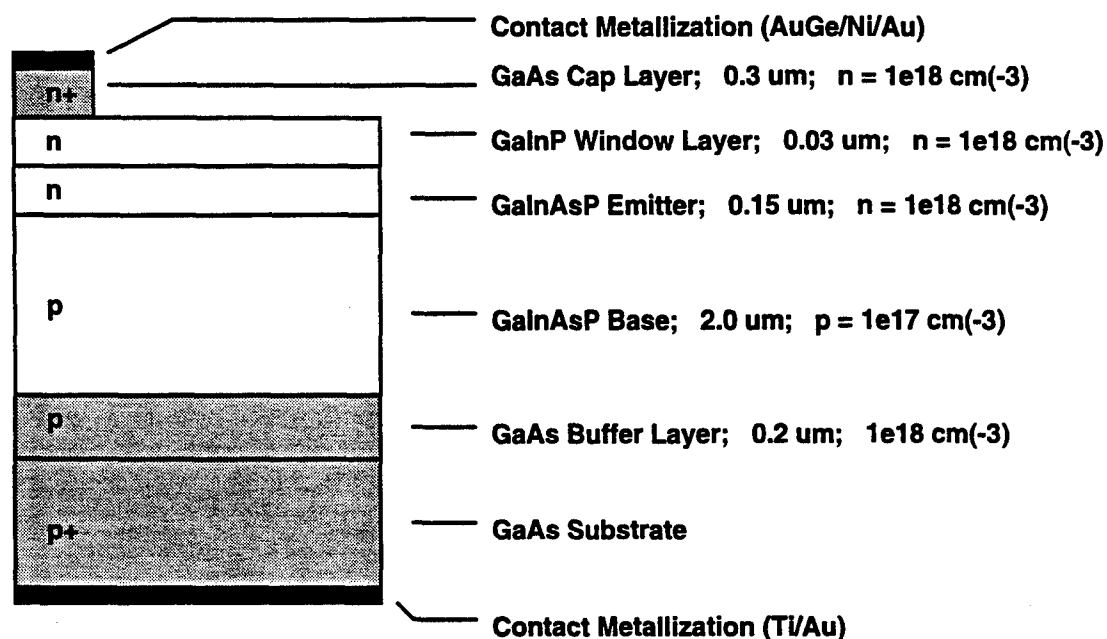
Figure 4.8. Basic structure of GaInAsP solar cells. This structure produced currents near program goals with little optimization.

The next series of cells began to show the promise that we believe GaInAsP has. The first of these, sample no. 6-568, yielded V_{oc}, J_{sc}, and FF values of 1.19 V, 19.3 mA/cm^2, and 0.83, respectively (values measured at ASEC), for an efficiency of more than 14 percent. After careful calibration of doping levels and growth rates to optimize the structures, the next cells provided ample reward for the efforts; a small-area cell was produced that significantly exceeded program goals. This cell, sample no. 6-628-6, produced an active-area efficiency of 21.5 percent (V_{oc}, J_{sc}, and FF of 1.161 V, 28.8 mA/cm^2, and 0.867, respectively). We believe that this was the first report of a quaternary cell achieving an AMO efficiency greater than 20 percent. The current from this cell is very close to what might be achieved theoretically. We asked ASEC to repeat the measurement to be certain of the simulator calibration, and the numbers were reproducible. We did measure the band gap using photoluminescence and found that the band gap was about 1.65 eV.

A series of these small cells were then used for radiation resistance measurements. The I-V characteristics before irradiation are shown in Table 4.6. Seven cells were used, and all had active-area efficiencies that ranged from 19.4 to 21.5 percent.

SPECTRAL RESPONSE

Ga$_x$In$_{1-x}$As$_y$P$_{1-y}$ Cell
w/AlInP$_2$ window

Al$_{0.2}$Ga$_{0.8}$As Cell
w/Al$_{0.7}$Ga$_{0.3}$As window
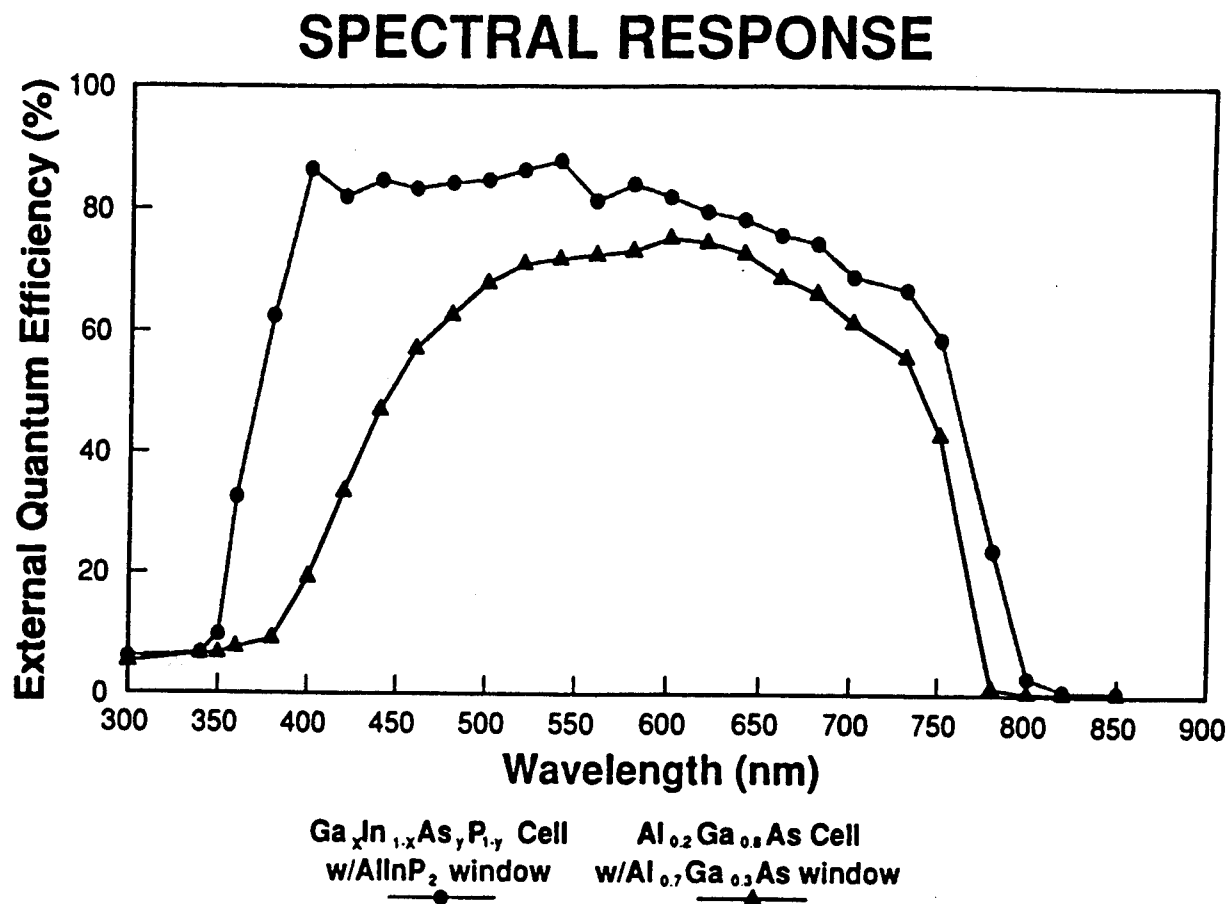
Figure 4.9. Spectral response characteristic of GaInAsP cell with an Al$_{0.5}$In$_{0.5}$P window layer compared to an Al$_{0.2}$Ga$_{0.8}$As cell with an Al$_{0.7}$Ga$_{0.3}$As window. The short wavelength response of the GaInAsP cell is markedly better.

Table 4.6.   Current-Voltage Characteristics of GaInAsP Solar Cells Before Irradiation.

Cell No.	V_{oc} (V)	J_{sc} (mA/cm^2)	FF (%)	η (%)
6-628-1	1.155	27.6	86.9	20.5
6-628-2	1.134	27.6	87.0	20.1
6-628-3	1.140	27.1	85.0	19.4
6-628-4	1.199	26.2	85.0	19.7
6-628-5	1.162	27.6	85.8	20.3
6-628-6	1.161	28.8	86.7	21.5
6-628-7	1.182	28.5	85.8	21.3
Averages	1.162	27.6	86.0	20.4

These are high-quality cells and prove that GaInAsP, as a material, has the potential to meet this program's needs. As noted above, these are small-area cells, fabricated for the radiation testing. We also produced cells with areas of 4 cm^2, one of the standard sizes for fitting into arrays. The data for two of these are shown in Table 4.7.

Table 4.7.   Current-Voltage Data for 4-cm^2 GaInAsP Solar Cells

Cell No.	V_{oc} (V)	J_{sc} (mA/cm^2)	FF (%)	η (%)
6-728	1.135	22.9	84.0	16.1
6-729	1.149	22.2	85.0	16.0

These efficiencies are total-area efficiencies. The most pleasing characteristic is the current because in both cells current densities exceed the 22-mA/cm^2 program goal. The current densities are slightly lower than the small-area cells. (The average active-area current density of the small cells is 27.6 mA/cm^2; correcting this for 7 percent grid obscuration gives 25.8 mA/cm^2. Also, the band gap of these cells was determined to be 1.68 eV, slightly higher than the 1.65 eV of the small cells, resulting in slightly less current.) Both of these cells, if combined with a Si cell capable of producing an effi-

ciency of 8 percent (BOL), would result in a stack that exceeds the 23 percent goal, assuming minimal interconnection losses.

With these data, combined with favorable radiation-resistance data to be described in the next section, the GaInAsP seemed, without doubt, capable of meeting program goals.

4.3.3 Radiation Testing of GaInAsP Cells

The GaInAsP cells whose I-V data are shown in Table 4.6 were irradiated with Si cells at the JPL facility under the direction of Dr. B. Anspaugh. The irradiation utilized 1-MeV electrons at a total fluence of 10^{15} cm^2. The pre- and post-irradiation data are shown in Table 4.8. The pre-irradiation data are identical to those presented in Table 4.6 and are repeated here to facilitate comparison.

The average EOL/BOL ratio of the efficiency for these seven cells is 0.79. The remarkable thing about this number is that these cells were not optimized in any way to enhance radiation resistance. For example, the carrier concentration in the bases are probably higher than the optimum value, and layer thicknesses have not been optimized. We think that with full optimization, it is not at all unrealistic to think that the EOL/BOL ratio for optimized GaInAsP junctions will be as larger. This is the level of performance that is needed for the total stack to have an EOL/BOL ratio of 0.8 since we expect the bottom cell to be slightly lower.

After testing, these cells were stored in a nitrogen dry box at room temperature. After three weeks, the I-V data were remeasured. The cells, according to the data, recovered some of the performance lost because of the irradiation. This type of low-temperature annealing is observed in InP but not in the arsenide compounds such as GaAs or AlGaAs. That the annealing behavior was observed in GaInAsP was a surprise, and we attribute the effect to the InP component of the ternary alloy. The magnitude of the effect does not seem to be as great as is observed in InP but would be an advantage of GaInAsP over AlGaAs, which shows little or none.

The result of remeasuring the cells was an average EOL/BOL that increased from 0.79 to 0.82. Excited by this result, the idea occurred that perhaps these cells might also show evidence of photon-assisted annealing, which is also observed with InP. The cells were placed under a simulator on a temperature-controlled block held at 28 °C in a short-circuit configuration. The cells were measured again after 16 hours of light soaking, and again performance improved. The average EOL/BOL ratio increased

50

Table 4.8.   Current-Voltage Characteristics of GaInAsP Solar Cells Before and After Irradiation With 1-MeV Electrons (10^{15} cm²).

Cell No.		V_{oc} (V)	EOL/BOL Ratio	J_{sc} (mA/cm²)	EOL/BOL Ratio	FF (%)	EOL/BOL Ratio	η (%)	EOL/BOL Ratio
6-628-1	Before	1.155		27.6		86.9		20.5	
	After	1.096	0.949	24.0	0.869	83.3	0.960	15.8	0.771
6-628-2	Before	1.134		27.6		87.0		20.1	
	After	1.080	0.952	24.4	0.885	83.2	0.955	16.2	0.807
6-628-3	Before	1.140		27.1		85.0		19.4	
	After	1.081	0.948	23.5	0.867	83.7	0.984	15.7	0.811
6-628-4	Before	1.199		26.2		85.0		19.7	
	After	1.129	0.942	23.2	0.885	83.6	0.984	16.2	0.822
6-628-5	Before	1.162		27.6		85.8		20.3	
	After	1.104	0.950	24.2	0.870	82.6	0.963	16.3	0.803
6-628-6	Before	1.161		28.8		86.7		21.5	
	After	1.080	0.930	24.0	0.830	82.3	0.949	15.7	0.732
6-628-7	Before	1.182		28.5		85.8		21.3	
	After	1.104	0.934	24.4	0.858	82.8	0.965	16.5	0.774
Avg.	Before	1.162		27.6		86.0		20.4	
	After	1.096	0.94	24.0	0.87	83.1	0.97	16.1	0.79

51

from 0.82 to 0.84. This test was followed with thermal annealing experiments, but no additional performance recovery was observed.

Nonetheless, we were delighted with what was observed. These GaInAsP cells recovered almost 24 percent of the initial performance loss caused by irradiation with 1-MeV electrons at a fluence of 10^{15} cm^{-2}. Test results are summarized in Table 4.9.

Again, it is worth pointing out that these cells were not optimized for radiation resistance, and greater EOL/BOL ratios are likely to result as the device and material system matures. These data also show that the Si cell will limit the tandem stack, not a new observation, but one with significant impact for this program.

Scientifically, it would be very interesting to study the low-temperature and photon-assisted annealing of these cells to identify the factors that enhance this phenomenon, but there was neither the time nor the resources for such a diversion.

4.4 Substrate Removal

The technique used for substrate removal depends on substrate material. For GaAs substrate, a solution of 19 H_2O_2; 1 NH_4OH provides a very convenient wet-chemical etchant because of its high selectivity for GaAs and very slow etch rates for $Al_xGa_{(1-x)}As$ with x values $\geq$ 0.7. Wet-chemical etching using this etchant was used in the early part of the program to fabricate stand-alone $Al_{0.2}Ga_{0.8}As$ layers that were sent to ASEC and used as filters to evaluate the realistic performance of Si cells as they would behave in the mechanical stack. This etching technique and solution are well-documented and are used in manufacturing processes, for example, for photocathodes.

The solutions were stirred during substrate removal, and etchants were held at room temperature. Usually the front surface of the layer or device was bonded to a quartz coverglass with a space-qualified adhesive. The coverglass then acts as a support for thin AlGaAs layers. Except for an occasional problem of seepage of the etchant between the adhesive and cell (resulted in etching of the front surface), this process works very well and could be used in large-number, batch processing. The time required to remove a substrate depends upon the GaAs thickness. We could typically remove a 250-μm-thick GaAs substrate in about 30 minutes. $Al_{0.8}Ga_{0.2}As$ was generally used as the stop-etch layer.

To remove Ge substrates, a dry-etching technique has been developed. The process is plasma-assisted and uses a mixture of CF_4/O_2 in the plasma discharge. This gas mixtures etches Ge extremely selectively compared to GaAs and leaves GaAs with very good surface morphologies. The etching rate depends on several parameters of the process, mainly the rf power, the chamber pressure, CF_4/O_2 ratio, and the total gas flow rate. These parameters are likely to vary from machine to machine. The equipment located at RTI is a small research-grade plasma system, but large commercial plasma reactors are commonly found in the Si integrated circuit industry.

Table 4.9. Current-Voltage Data For GaInAsP Solar Cells Showing Recovery From Radiation-Induced Damage.

Cell No.	Voltage Recovery (V)				Current Recovery (mA/cm^2)				Efficiency Recovery (%)			
	Voc0	Voc1	Voc2	Voc3	Jsc0	Jsc1	Jsc2	Jsc3	Eff0	Eff1	Eff2	Eff3
6-628-1	1.155	1.096	1.113	1.121	27.6	24.0	24.3	24.7	20.5	16.2	16.7	17.4
6-628-2	1.134	1.080	1.098	1.105	27.6	24.4	24.7	25.1	20.1	16.2	16.7	17.3
6-628-3	1.140	1.081	1.105	1.116	27.1	23.5	23.8	24.6	19.5	15.7	16.2	17.0
6-628-4	1.199	1.129	1.146	1.153	26.2	23.2	23.8	24.3	19.8	16.1	16.8	16.9
6-628-5	1.162	1.104	1.121	1.128	27.6	24.2	24.3	24.7	20.3	16.1	17.0	17.5
6-628-6	1.161	1.080	1.094	1.103	28.8	24.0	24.3	24.7	21.5	15.7	16.2	16.8
6-628-7	1.182	1.104	1.119	1.125	28.5	24.4	24.7	24.7	21.3	16.5	17.0	17.6
Avg.	1.162	1.096	1.114	1.122	27.6	24.0	24.3	24.7	20.4	16.1	16.7	17.2
EOL/BOL	—	0.94	0.96	0.97	—	0.87	0.88	0.90	—	0.79	0.82	0.84

Notes:
1. Voc0, Jsc0, and Eff0 measured before irradiation.
2. Voc1, Jsc1, and Eff1 measured immediately after irradiation.
3. Voc2, Jsc2, and Eff2 measured after 3-week storage in room-temperature dry box at open circuit.
4. Voc3, Jsc3, and Eff3 measured after 16-hour light soaking under AM0 simulator at 28°C at short circuit.
5. Changes in fill factor were small compared to other parameters and are not included above.

Therefore, scale-up of this process should be both relatively easy and cost effective. This process is certain to be compatible with the manufacturing environment.

4.5 Summary of AlGaAs and GaInAsP Results

To summarize the effort expended on the AlGaAs and GaInAsP high-band-gap cells, it is fair to say a substantial amount of progress was made. GaInAsP cells with the necessary composition to provide the needed 1.7-eV band gap were demonstrated, and these cells have the following characteristics:

- Efficiencies exceeded 20 percent—a first for a quaternary cell, we believe.

- EOL/BOL efficiency ratios are about 0.8 immediately after irradiation with 10^{15}, 1-MeV electrons/cm^2.

- Cells show low-temperature injection annealing; cells recovered about 24 percent of the pre-irradiation performance, yielding an EOL/BOL ratio of 0.84—also a first-time observation for a quaternary cell.

In short, this material and these cells look very promising for devices to be used in space.

$Al_{0.2}Ga_{0.8}As$ cells were very close to performance expectations using p/n polarities, but radiation resistance and BOL efficiency of the Si bottom cell dictated that the n/p polarity be developed. Although modeling showed that the performance of the two polarities should be similar, n/p $Al_{0.2}Ga_{0.8}As$ never achieved cell currents that would allow goals to be met. $Al_{0.2}Ga_{0.8}As$ cells grown in the program's last gasp with an improved TMA source failed to perform well because of unresolved structural problems.

At the end of Phase I in the program, the decision was made to focus on $Al_{0.2}Ga_{0.8}As$ instead of GaInAsP. This decision was based primarily on perceived ease of manufacturing of AlGaAs compared to GaInAsP, on more difficult composition control of GaInAsP, on cost of organometallic source materials, and the well-developed wet chemistry of AlGaAs needed in device processing. In view of the difficulties that were encountered with AlGaAs, the inordinately large amount of program resources expended to achieve performance goals with AlGaAs, and the progress of other phosphide-based materials such as GaInP (in the GaInP/GaAs tandems), this decision, in hindsight, should have gone the other way. While reversing the decision would not have eliminated the radiation resistance problems of a Si bottom, the top cell difficulties might have been far smaller. Perhaps an old saying should have been modified for this program: "*A GaInAsP bird in the hand is worth two AlGaAs birds in the bush.*"

5.0   METAL BONDED INTERCELL CONNECTION

5.1   Introduction

Connecting an AlGaAs (or GaInAsP) top cell that is only several micrometers thick to a thin Si bottom cell was not expected to be a trivial task. The results that were obtained during the program confirm that this is, indeed, the case. However, the data that were generated do suggest the technique of metal bonding of the two cells is viable. This conclusion is based on mechanical and electrical considerations. Optical considerations, the third requirement of the interconnect, were scheduled for Phase 3, which was not funded.

In this section, we describe the means of forming the mechanical interconnect, analysis of the losses, and characterization of interconnects.

5.2   Formation of Metal Bonded Interconnects

Intercell bonding in the type of structure being developed here must provide good mechanical adhesion and low electrical and optical losses. The general approach taken by RTI and ASEC is to metallize one or both surfaces of the materials that are to be joined. The pieces are then placed in intimate contact and pressure is applied. The pieces are then heated. At some temperature, hopefully a reasonably low one, the metals intermix and/or form alloys with the semiconductors that are being joined. The matching surfaces must be flat, as would be the surface of a top cell after removing the substrate and regions of a Si wafer that have not been textured. The bond must not produce residual strain that can degrade device performance.

In RTI's approach to bonding GaAs to Si, described in Ref. 3, thin metal layers of Sn-Au-Sn were applied to Si, and a GaAs layer grown on a Ge substrate was bonded to the metal-covered Si surface. The metal stack forms eutectic alloys with both Si and GaAs at temperatures close to 300°C. The formation of these eutectic alloys provides the strength of the bond. After bonding, the Ge substrate was removed with dry, plasma-assisted etching. The resulting structure produced a minority-carrier lifetime of more the 100 ns and demonstrated Fabry-Perot action for sub-band-gap wavelengths. This minority-carrier lifetime is the longest for any GaAs layer bonded to Si that we are aware of, and the Fabry-Perot cavity action indicates that the interface between the Si and GaAs is very smooth and highly reflective. Raman spectroscopy performed on the GaAs layer revealed no evidence of residual strain, which is an important observation.

ASEC examined other metals, including Au, Pd, An, Nb, and Ti, and found that Pd gives strong adhesion to both GaAs and Si at fairly low temperatures (below 400°C).

One of the goals of these efforts was to reduce the bonding temperature as much as possible to reduce thermal stressing that cannot be avoided during cooling.

ASEC used a tic-tac-toe-shaped grid to evaluate the strength of the mechanical connection. Using 2×2 cm^2 pieces of GaAs and Si, grids were aligned in one direction on the GaAs and perpendicular to that on the Si. The overlap area of the grids is estimated to be about 10^{-3} cm^2. After bonding, the stack was transferred repeatedly between boiling water and liquid nitrogen. No evidence of delamination could be found. This experiment, besides showing the resiliency of the interconnect, also suggests that a pattern of small dots or squares could be used as effectively instead of lines.

Most of the experiments to develop interconnects used thick pieces of GaAs and Si. However, RTI did use the technique to bond thin layers of AlGaAs to Si. Ge substrates, upon which the AlGaAs had been grown, were removed. This structure is a proof-of-concept that the proposed devices can be made. Our major concerns about the structure are the cost and yield if this process were transferred out of research and development to a manufacturing environment.

In summary, then, the method of forming this type of intercell connection is essentially this: A "sandwich", consisting of the two semiconductor parts to be joined and metal layers between the semiconductors, is made. This stack is heated under mechanical pressure until the metals and the semiconductor intermix, forming continuous alloy mixtures. The amount of pressure required and the bonding temperature varies with the semiconductor and metals being used and must be optimized empirically.

5.3   Analysis of Interconnect Losses and Optical Considerations

Figure 5.1 gives a schematic representation of the mechanically stacked tandem solar cell that was developed for this program. S and W are the grid spacing and width, respectively. This design consists of evenly spaced, narrow grid lines that lie beneath the front surface grid metallization to minimize shadowing losses. Several assumptions were made to complete the analysis of the losses. They are:

- Because current flow is vertical in the structure, no grid line losses for the interconnect are assumed, i.e. there is no current flow along the interconnect.

- Both facing surfaces are assumed to have sheet resistances ρ_{SH} of 50 Ω/sq, not unreasonable for a diffused Si cell with surface concentration greater than 10^{20} cm^{-3} and a very heavily doped III/V layer.

- Grid line width W is assumed to be 0.005 and 0.010 cm in two analyses.

- The grid spacing S is used as a parameter.

- Specific contact resistivities (ρ_c) of 10^{-2} and 10^{-3} ohm-cm^2 are assumed to optimize S, and the effect of reducing ρ_c to 10^{-4} ohm-cm^2 is then examined.
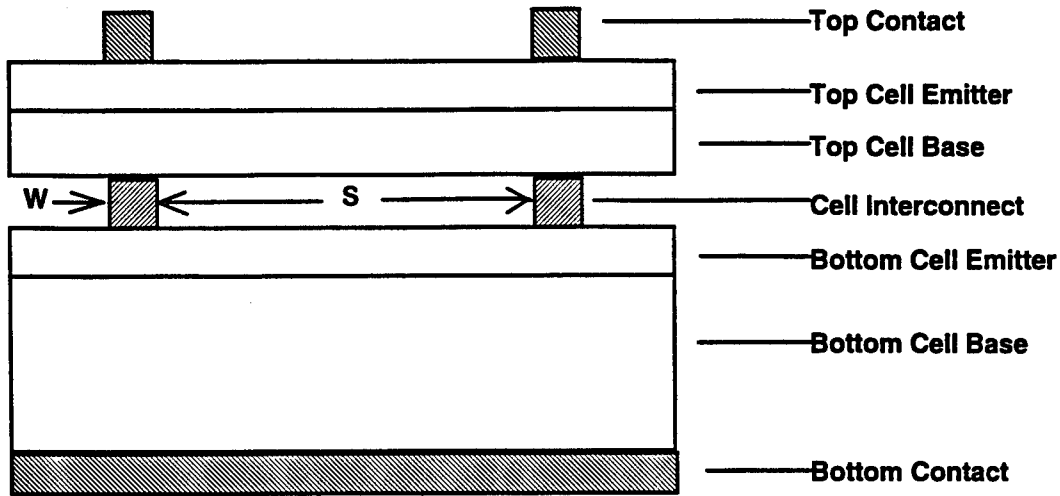
Figure 5.1. Schematic cross-section of mechanically stacked tandem solar cell. S is the spacing of the interconnect grid, and W is the grid line width. The top cell is a very thin (5 μm) AlGaAs or GaInAsP junction. The bottom cell is made of Si.

The interconnect has three main loss sources: sheet resistance (doubled to account for both surfaces); contact resistance (also doubled to account for both surfaces); and shadow loss. The loss terms can be expressed as a fraction of the impedance of the cell at the operating point. For the devices under development we expect V_{max} to be about 1.5 V, and I_{max} of 20 mA/cm^2, or an internal impedance of about 75 ohms.

There is an obvious trade-off. As the grid spacing is reduced or the grid width is increased, sheet and contact losses, respectively, will decrease, but shadow losses will increase. Hence, we are looking for the value of S that minimizes the sum of the three loss terms. Following an analysis for linear grids presented by Moore [5], the fractional losses are expressed as:

$$F_{SR} \approx \frac{(2I_{max}\rho_{SH}S^2)}{12V_{max}} = 0.112S^2,$$

$$F_C \approx \frac{(2I_{max}\rho_C)S}{WV_{max}} = 0.005S, \text{ and}$$

$$F_S = \frac{W}{S} = 0.005 / S,$$

where F_{SR}, F_C, and F_S are, respectively, the fractional spreading resistance, contact resistance, and shadowing losses. The sum of these three terms approximates the total interconnect loss. Differentiating this sum with respect to S and setting the result equal to zero gives the minimum value of S. With the stated conditions, the minimum value of S is about 0.28 cm, or between 3 and 4 grid lines per cm.

What is not included in this analysis are the reflective losses that will occur at the interfaces where the two cells join. Minimizing this loss requires good antireflective coatings on both semiconductor surfaces. More will be said about optical considerations below.

The results obtained by solving the three loss equations for a range of S values are shown in Table 5.1. These data show that the minimum loss occurs at 0.2 cm < S <0.35 cm, in good agreement with the differentiation described above.

Table 5.1. Fractional and Total Losses as a Function of Grid Spacing.

S (cm)	F_{SR} (%)	F_s (%)	F_C (%) $\rho_c=10^{-2}$ (ohm-cm^2)	F_C (%) $\rho_c=10^{-3}$ (ohm-cm^2)	Total Losses (%) $\rho_c=10^{-2}$ (ohm-cm^2)	Total Losses (%) $\rho_c=10^{-3}$ (ohm-cm^2)
0.05	0.03	10.0	0.27	0.03	10.3	10.1
0.15	0.25	3.30	0.81	0.08	4.36	3.63
0.20	0.45	2.50	1.10	0.11	4.05	3.10
0.25	0.70	2.00	1.35	0.14	4.05	2.80
0.35	1.38	1.40	1.90	0.19	4.70	3.00
0.45	2.28	1.10	2.43	0.24	5.81	3.62
0.70	5.50	0.70	3.80	0.38	10.0	6.60
0.90	9.00	0.6	4.90	0.49	14.5	10.1

From the data in Table 5.1, we surmise that even for very modest contact resistivities of 10^{-2} ohm-cm^2, the total nonreflective losses are below 5 percent, the program goal, with appropriately spaced grids. The trends in the loss data become more apparent in graphical form, shown in Figure 5.2. It is also worth noting that with the optimum

value of grid spacing, very little is gained by trying to push the interface resistivity below 10^{-3} ohm-cm^2. This, in fact, would be an exercise of diminishing returns.
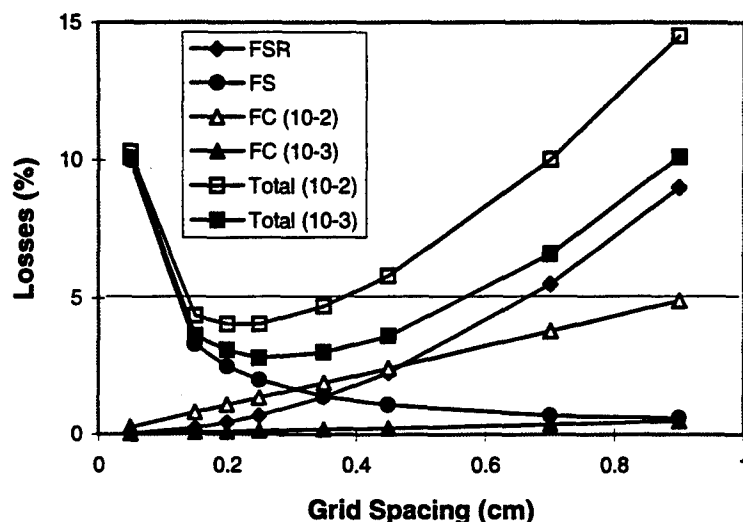

Figure 5.2. Results of loss analysis for metal interconnects joining AlGaAs and Si solar cell. Contact resistivities of 10^{-2} and 10^{-3} ohm-cm^2 have been assumed. F_{SR}, F_s, and F_c are sheet resistance, shadowing, and contact resistivity losses, respectively. Five percent loss, the program goal, is indicated on the chart.

The analysis is also useful in showing the importance of producing minimum reflectance at the two facing surfaces for the wavelengths that are not absorbed in the top cell. With no AR coating on either of these surfaces, the reflectance would be greater than 30 percent at each surface, and this loss would prevent the cells from generating equal currents. In the final structure, we planned for the Si bottom cell to have low reflectance, produced by a combination of textured surface and an AR coating optimized to the relatively narrow band of wavelengths between 730 nm to 1,100 nm, the band-edge of Si.

It is essential to apply a similar AR coating to the back of the top cell.

The AR coatings must be completed during metallization of the surfaces that are to be joined since that interface will, obviously, no longer be available for processing after bonding.

Even with the appropriate AR coatings in place, it may be necessary to fill the thin gap between the cell, typically a few μm, with a dielectric layer. Reflections can conceivably be reduced to about 1 to 2 percent with all components optimized at the interface. Adding the resistive losses to the reflective losses gives a best-case loss of between 5 and 7 percent for the bonded interconnects.

5.4   Measurement of Interconnect Resistivity

To test the range of resistivities that could be obtained from the metal intercon-nect, particularly in view of the previous analysis, a test structure was fabricated. The test structure contained a 300-μm-thick, n-type GaAs wafer and a 200 μm-thick Si piece, also with n-type conductivity. The top of the GaAs was metallized with AuGe/Ni/Au layers, which provides an ohmic contact to the top surface, and the bottom of the Si received a Ti/Pd/Au contact that was ohmic but fairly resistive. These pieces were joined with Au/Sn/Au metallization that covered about 15 percent of the interface surface.

The specific contact resistivity of the entire structure was measured, and a value of 4.2×10^{-2} ohm-cm^2 was obtained. This is the total resistivity of the bonded structure. With respect to the interconnect, it would be a "worst case" value since it contains con-tributions from bulk resistivity of the two wafers, which should be small, and contact re-sistivity. The contact resistivity of the AuGe/Ni/Au to GaAs is typically less than 10^{-4} ohm-cm^2 and probably makes little contribution. Although not measured, the resistivity to the Ti/Pd/Au contact was high because the Si wafer was lightly doped. This resistiv-ity definitely made an impact on the measurement. By the same token, the resistivity of the bonded connection to Si was probably high because of the same low carrier con-centration in the Si wafer.

The contact resistivity to the GaAs (assuming a thin layer of heavily doped, p-type GaAs is grown on the bottom of the AlGaAs top cell to reduce contact resistivity) was estimated in summer work funded at JPL by ASEC. JPL workers used a multiple-metal stack of Ti (300 Å), Au (3000 Å), and Ag (1000 Å) to contact the GaAs. This metallization scheme usually produces good ohmic connection to GaAs without alloying if p-type carrier concentrations are sufficiently high. However, the contact was sub-jected to the heat treatment thought necessary to form the metal bond between the top and bottom cells. Data, using the transmission line model (TLM), were then measured. Contact resistivities for this process ranged from a low of 2.1×10^{-5} to 4.8×10^{-4} ohm-cm^2. These numbers are well below the 10^{-3} program goal and show that this portion of the contact should not limit the total interconnect resistivity.

In short, we believe that attaining an electrical resistivity less than 10^{-2} ohm-cm^2 , as is indicted to be necessary by the analysis described above, is absolutely within the realm of what is pragmatically achievable. This further suggests at from a resistivity point-of-view, the metal bonded interconnect is a viable means of joining two materials. Reduction of optical losses appears now to be far more challenging.

6.0 CONCLUSIONS AND RECOMMENDATIONS FOR FUTURE RESEARCH

6.1 Conclusions

There are several conclusions that can be drawn from this body of work. They are the following:

1. While the Si solar cell has been the work horse of photovoltaic devices, it is being replaced by devices that have higher efficiencies and more resistance to radiation damage. To include Si in a tandem structure truly accentuates the radiation "softness", discussed for the first time in this work, in the spectral region of $\lambda \geq 0.73 \ \mu m$.

2. This problem in Si can be ameliorated by using thin cells made of high-resistivity material, but this cell weakness was not eliminated in the efforts described herein and would have made program radiation goals difficult to achieve.

3. The BOL efficiencies for the Si cells must be very high to achieve the modeled stack efficiency goal.

4. The metal interconnection using metal bonding has been shown to be a viable means of joining two cells using specific contact resistivity as the determining criterion. Optimization of the optical characteristic requires careful attention. The interfaces during this program were not rigorously optimized, but optical losses were estimated to be only 5 to 15 percent. This bodes well for the potential of the interconnect in this and other applications.

5. AlGaAs remains the elusive entity at the end of the program that it was at the beginning, particularly for the n/p cell configuration. A good deal of understanding of the characteristics for problems have been developed, but workable solutions are still not positively identified. An improved source of TMA, the dominant Al source in OMVPE technology, has been identified, but structural problems with devices grown at the end of the effort kept, we believe, improved cells from being manufactured.

6. Finally, GaInAsP turned out to be the surprising "star" of the program. Not only were high efficiencies greater than 20 percent achieved, a first for a quaternary III/V material, but both radiation resistance and room-temperature annealing of radiation-induced damage were demonstrated.

This research conducted under this funded effort has also contributed to the body of scientific knowledge. Various aspects of the effort were described in three papers that were accepted and presented at the 23rd and 24th IEEE Photovoltaic Specialists Conferences and one paper at the Space Power Workshop.

6.1   Recommendations

Making recommendation from this body of work is straightforward because the suitable topics are obvious.

Clearly, the most outstanding result was the work with GaInAsP. We believe this material, like GaInP, is an outstanding material for space applications. While work with GaInAsP was curtailed prematurely because of perceived, but unproved, manufacturing considerations, we think the progress made in a relatively short period of time makes the material an obvious candidate for future research.

We also believe that the metal interconnect is a viable means of joining solar cells and producing a two-terminal device. It would be better if the top cell were not so thin, i.e., manufacturing yields will be higher and processing simpler. This approach may be the only pragmatic means of joining two cells with widely different lattice constants to achieve optimum band gaps in multiple-cell structures.

Finally, high-quality AlGaAs solar cells remain attractive, elusive, and perhaps unattainable (by OMVPE) in a manufacturing environment because of the chemical reactivity of Al and deep levels such as the DX center. If it can be made to work, its advantages are, as noted in the body of the work, powerful. We must admit to what appears to be a prejudice toward AlGaAs that may color our opinion about its worth.

7.0 REFERENCES

1. Bertness, K.A., Kurtz, S.R., Friedman, D.J., Kibbler, A.E., Kramer, C., and Olson, J.M., "High Efficiency GaInP/GaAs Tandem Solar Cells for Space and Terrestrial Applications," *Proceeding of the 1st WCPEC* (IEEE Press, NJ, 1995) pp. 1671-1678.

2. Private Communication with Dr. T. Coutts, National Renewable Energy Laboratory, Golden, CO.

3. Venkatasubramanian, M.L. Timmons, T.P. Humphreys, B.M. Keyes, and R.K. Ahrenkiel, "High-Quality Eutectic-Metal-Bonded AlGaAs-GaAs Thin Films on Si Substrates," *Appl. Phys. Lett.*, **60**, pp. 886-888 (1992).

4. Yamaguchi, M., "Radiation Resistance of Compound Semiconductor Solar Cells," *J. Appl. Phys.*, **78** (3), pp. 1476-1480 (1 August 1995)

5. Moore, A.R., "An Optimized Grid Design for a Sun-Concentrator Solar Cell," *RCA Review*, **Vol. 40**, pp.140-165 (June 1979).

DISTRIBUTION LIST

AUL/LSE
Bldg 1405 - 600 Chennault Circle
Maxwell AFB, AL 36112-6424   1 cy

DTIC/OCP
8527 John J. Kingman Rd, Suite 0944
Ft Belvoir, VA 22060-6218   2 cys

AFSAA/SAI
1580 Air Force Pentagon
Washington, DC 20330-1580   1 cy

PL/SUL
Kirtland AFB, NM 87117-5776   2 cys

PL/HO
Kirtland AFB, NM 87117-5776   1 cy

Official Record Copy
   PL/VTP/Lt Keener   2 cys
Kirtland AFB, NM 87117-5776

PL/VT   1 cy
Dr Wick
Kirtland AFB, NM 87117-5776